SKB

TECHNICAL REPORT

97-09

A regional analysis of groundwater flow and salinity distribution in the Äspö area

Urban Svensson

Computer-aided Fluid Engineering AB

May 1997

A REGIONAL ANALYSIS OF GRUNDWATER FLOW AND SALINITY DISTRIBUTION IN THE ÄSPÖ AREA

Urban Svensson

Computer-aided Fluid Engineering AB

May 1997

A REGIONAL ANALYSIS OF GROUNDWATER FLOW AND SALINITY DISTRIBUTION IN THE ÄSPÖ AREA

Urban Svensson

Computer-aided Fluid Engineering AB

May 1997

ABSTRACT

A regional groundwater model of the Äspö area has been formulated and applied. The model is three-dimensional, based on a grid of $100 \times 100 \times 36$ cells and covers an area of 10×10 km^2 and a depth of 3 km. Equations are solved for the Darcy velocities, mass conservation and the salinity distribution; gravitational effects are thus fully accounted for.

The model is used to simulate the general hydrology of the area (infiltration, run-off, saltwater penetration, etc.) as well as the influence of the Äspö HRL. A specific task of the study is to evaluate relevant boundary conditions for a site-model and to show how these are influenced by Äspö HRL. Also specific studies of the stochastic conductivity field and the effect of density stratification are reported.

The general conclusion from the study is that the model provides a realistic and consistent picture of the area studied. The main arguments for this statement are:

- The mathematical formulation of the model is based on relevant conservation laws and embodies all physical processes believed to be important for the problem considered. The importance of gravitational forces is in this context emphasised.

- A high resolution grid, which resolves topographical features and at the same time can simulate the effect of the Äspö HRL, is used.

- Transmissivities and conductivities used in the model are based on field data.

- The model has been calibrated, using measured groundwater levels and salinity distributions, with good result.

- A range of sensitivity studies has been carried out. These demonstrate that the model responds to variations in input data, for example the conductivity field, in a realistic way.

The model can thus be used to generate boundary conditions for a site scale model. The basic objective, to account for the regional influence in a site model, can hence be achieved.

ABSTRACT (Swedish)

En regional grundvattenmodell över Äspö-området har formulerats och tillämpats. Modellen är tredimensionell, det numeriska beräkningsnätet innehåller 100 x 100 x 36 celler och täcker en yta av 10 x 10 km^2 och ett djup av 3 km. Ekvationer löses för Darcy-flöden, masskonservering och transport av salt. Gravitationella effekter beaktas genom att densiteten är en funktion av salthalten.

Modellen simulerar de centrala hydrologiska processerna i området (infiltration, avrinning, saltvatteninträngning under land, etc) och även effekten av Äspölaboratoriet. Detta är ett av huvudsyftena med modellutvecklingen. Ett annat är att generera relevanta randvärden för modeller som täcker ett mindre område runt Äspö; detta både för naturliga förhållanden och med Äspölaboratoriet. Rapporten redovisar också känslighetsstudier med avseende på hydrauliska konduktivitetsfältet och effekten av densitetsskiktning.

Den generella slutsatsen från arbetet är att den utvecklade modellen ger en realistisk bild av den allmänna hydrologin i området. Denna slutsats baseras på följande argument:

- Den matematiska formuleringen av modellen baseras på relevanta konserveringslagar och inkluderar alla väsentliga fysikaliska processer. Effekten av gravitationella krafter är en sådan väsentlig process.

- Ett högupplösande beräkningsnät används för att samtidigt kunna beskriva topografin i området och inflytandet av Äspölaboratoriet.

- Transmissiviteten och konduktiviteten som används i modellen baseras på värden som erhållits från fältmätningar.

- Modellen har kalibrerats med hjälp av uppmätta grundvattennivåer och salthaltsfördelningar.

- Sensitivitetsstudier visar att modellen reagerar på ett rimligt sätt på variationer i t.ex. materialspecifikationen.

Modellen kan således användas för att generera randvärden till en lokal modell för Äspöområdet och därmed inkludera regionala effekter i en modell för ett mindre område runt Äspö.

TABLE OF CONTENTS

1 INTRODUCTION

The Äspö Hard Rock Laboratory (HRL) is a laboratory for the development and testing of methods for detailed characterisation of the rock volume from excavated tunnels. Further, Äspö is a full scale laboratory for testing construction and handling techniques and for the demonstration of important parts of a repository system. Finally, it provides a multitude of data for development of our knowledge of important processes in deep crystalline bedrock and for testing of models for groundwater composition, groundwater flow and radionuclide migration.

A major milestone was reached 1996 with the completion of the pre-investigation and construction phases. The comprehensive research conducted has enabled valuable development and verification of site characterisation methods applied from the ground surface, boreholes and underground excavations. The hydrogeological characterisation of the area has in this context been revised and updated, see Rhén et al (1997). The updated conceptual models and data have motivated the present study and will form the basis for the numerical simulations to be presented.

In the safety assessment of a deep repository for spent nuclear fuel, it is expected that numerical simulation models will play an important role. The models can provide estimates of the groundwater flow around the repository and transport times, from the repository to the biosphere, for tracers. One of the problems when setting up such models concerns scales. We need to consider length scales from 10 metres (canister performance) to a regional scale of perhaps 10 km. Most of the models have so far been set up for a site scale, which typically covers a volume of $1 \times 1 \times 1$ km^3. At the vertical boundaries of the site scale model one needs to assume that the pressure and salinity distributions are known. Generally, it is not possible to account for a regional groundwater flow by these boundary conditions. The site scale model is used to analyse, for example, a pumptest or the impact from a tunnel. Once again we have a problem with boundary conditions, as we can do no better than assume that the boundary conditions are not significantly altered by the pumptest or the tunnel.

The objective of the study is to increase our understanding of the regional groundwater flow in the Äspö area. It is also expected that a regional groundwater model can provide more realistic boundary conditions for a site scale model. The study is site-specific as we
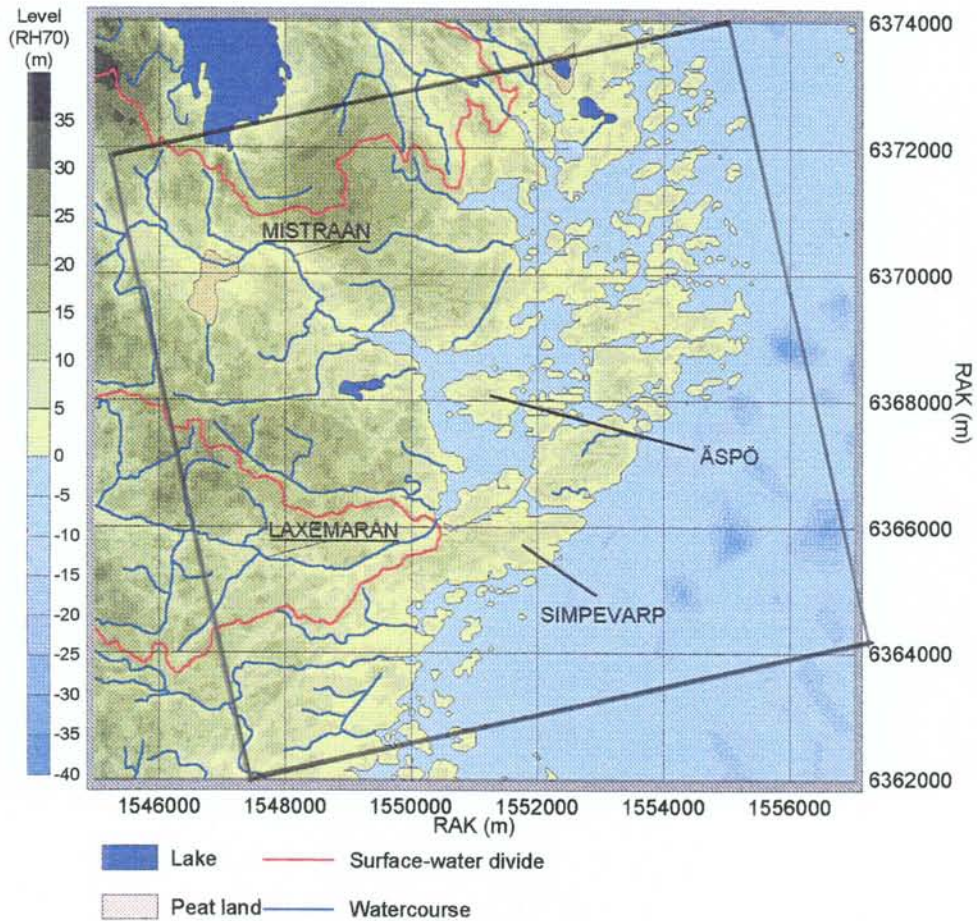
Figure 1-1. *The area considered in the regional model. The black square indicates the model area (10 x 10 km²) oriented in the Äspö coordinate system.*

focus on an area of 10 x 10 km², centred around the island of Äspö, see Figure 1-1.

A literature survey indicates that few regional model studies of coastal areas, i.e. where density stratification is essential, have been performed. The generic problem of the salt/fresh water interface is treated in textbooks, see de Marsily (1986) and Bear and Verruijt (1987). The modelling of groundwater-brine systems is reviewed by Oldenburg and Pruess (1995). In this paper the computational problems associated with large (> 5%) density variations are discussed. Ghassemi et al (1996) simulate seawater intrusion in a coastal aquifer. The problem considered by Ghassemi et al (1996) has several similarities with the regional flow to be discussed in this report. A conclusion from the paper is that "supercomputing facilities become inevitable if the problem is not a small-scale one". The present report will show that this is not always the case.

2 GENERAL DESCRIPTION OF THE AREA

The area considered, see Figure 1-1, is at the border of the Baltic Sea. The salinity of the Baltic Sea is about 0.6% in the area around Äspö and it is known from boreholes on Äspö that the salinity increases with depth below Äspö and hence most likely also under the Baltic. We can thus expect sea water to be found in under land, according to the classical Ghyben-Herzberg principle.
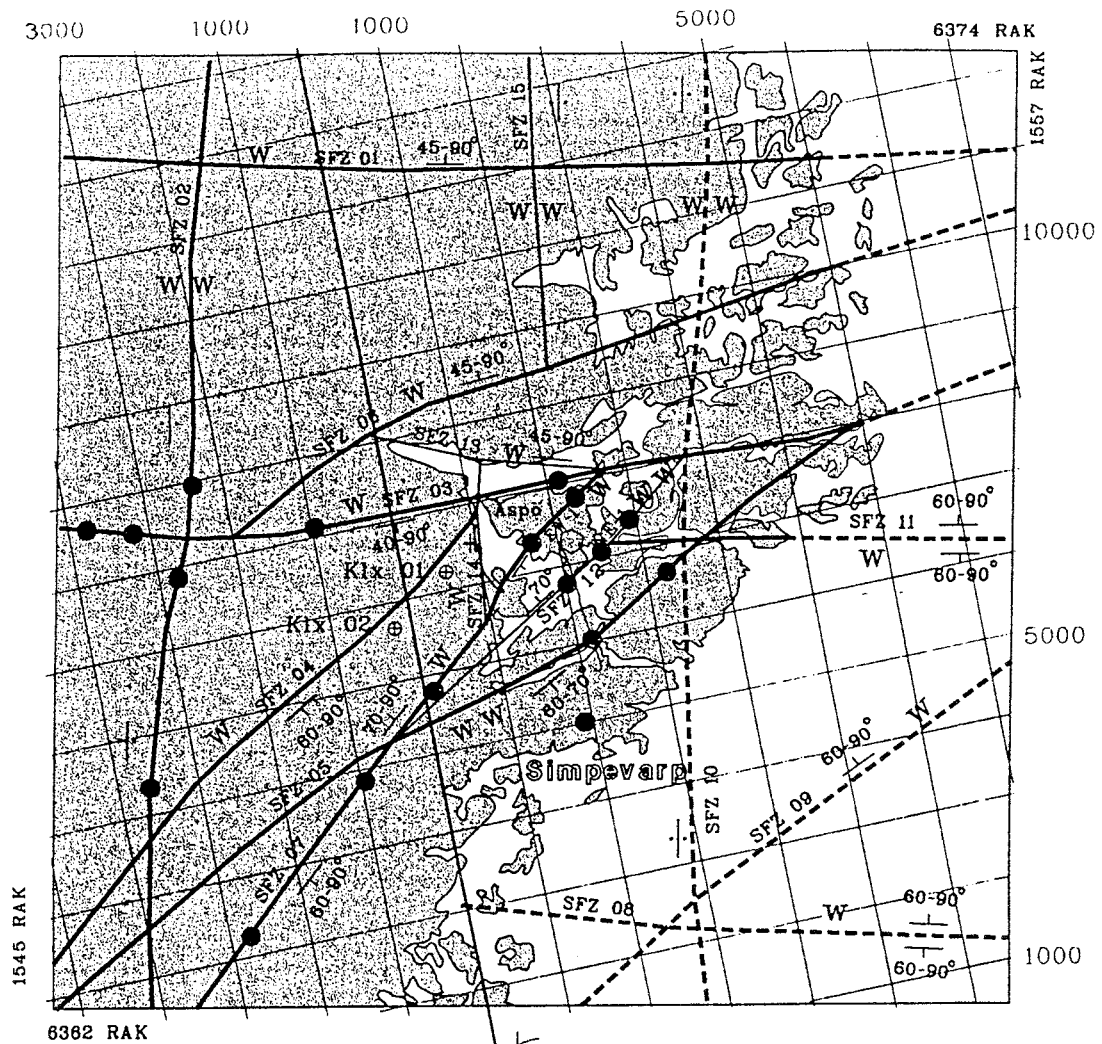
The topography of the area is gentle with small hills with a maximum elevation of about 30 metres above the sea level. The soil cover is thin (0-5 m) and the area is forested mainly with pine forest.

Mean precipitation minus evapotranspiration, P-E, has been estimated to be about 200 mm/year. The drainage system for the region is given in Figure 1-1, where surface water divides and small rills and channels are marked. Laxemarån and Mistraån are the two most important rivers in the area.

The major transmissive fracture zones in the region are shown in Figure 2-1. The transmissivities have been estimated, see Rhén et al (1997), to be 0.3×10^{-5} m^2/s (W) and 10.0×10^{-5} m^2/s (WW). Hydraulic conductivities at different depths for the rock inbetween the fracture zones have been estimated from field measurements, see Rhén et al (1997). It is well-known that these conductivities, and their standard deviations, vary with the testscale. When a numerical model is set-up one needs to consider the relation between the cell size in the grid and the testscale. The values given in Table 2-1 represent a testscale of 100 metres, which is also the cell size in the numerical model. The values for depth > 600 metres are however strictly for a testscale of about 300 metres. For further details about scaling laws and details about the field measurements, see Rhén et al (1997).

Table 2-1. Rockmass hydraulic conductivity and its standard deviation for the region considered. After Rhén et al (1997).

Depth (m)	K (m/s)	s ($\log_{10}$ K)
0 - 200	1.3 E-7	0.96
200 - 400	2.0 E-7	0.65
400 - 600	2.6 E-7	0.79
600 →	4.7 E-8	0.72

Figure 2-1. Major fracture zones in the area, after Rhén et al (1997). (Coordinate systems: RAK and Äspö).

3 NUMERICAL SIMULATION MODEL

3.1 BASIC APPROACH AND ASSUMPTIONS

Regional groundwater models can be developed for a number of purposes; perhaps the most common one is that the rainfall - runoff relation is requested. As stated above, the objective of the present study is to understand the regional groundwater flow below the island of Äspö. With this in mind the following basic requirements for the simulation model have been formulated:

- It needs to be three-dimensional with high resolution in space. We need to be able to simulate the effect of the Äspö Hard Rock laboratory (HRL) and at the same time resolve the general hydrology of the regional area.

- Variable density needs to be accounted for, as the salinity of the groundwater will vary in the domain.

- The model should predict a realistic groundwater table, as we expect a balance between the pressure generated by the water table and the pressure due to the internal density distribution.

We will further introduce some basic assumptions; some of which are motivated by the purpose of the study, others by the lack of information or data. The following assumptions are made:

- Flow, pressure and salinity fields are in a steady state. This assumption seems appropriate from the purpose of study. It may however be questioned if the salinity field will ever be in a steady state.

- Spatial uniformity. Due to lack of data we need to assume that precipitation and evapotranspiration are horizontally uniform. Variations in land use, vegetation or soil types are also neglected.

- The unsaturated zone can be handled by the simple algorithm introduced in Svensson (1995).

The computational domain was introduced in Figure 1-1. The motives for the size and orientation of the domain can be summarised as follows:

- The orientation should follow the Äspö coordinate system, for simple and secure integration with the Äspö data base.

- The test-scale for the hydraulic conductivities was 100 metres, which is a strong argument for a cell-size of about 100 metres.

- The computational grid should not have more than 500 000 cells, in order to avoid extreme execution times on a low-end workstation.

These considerations led to a domain of 10 x 10 x 3 km^3, centred around the island of Äspö, represented in a computational grid of 100 x 100 x 36 cells.

These are the basic requirements and assumptions of the model.

3.2 MATHEMATICAL FORMULATION

For the momentum balance it will be assumed that the Darcy law applies. For the salinity equation we will assume a balance between advective transport and dispersion, i.e. the time derivative is neglected.

Within these assumptions, and the ones in the previous section, the following set of equations can be formulated.

Momentum:

$$0 = -\frac{\partial p}{\partial x} - \frac{\rho g}{K_x} u \qquad (1)$$

$$0 = -\frac{\partial p}{\partial y} - \frac{\rho g}{K_y} v \qquad (2)$$

$$0 = -\frac{\partial p}{\partial z} - \frac{\rho g}{K_z} w - \rho g \qquad (3)$$

Salinity balance:

$$\frac{\partial}{\partial x} us + \frac{\partial}{\partial y} vs + \frac{\partial}{\partial z} ws = \frac{\partial}{\partial x}\left(Dn\frac{\partial s}{\partial x}\right) + \frac{\partial}{\partial y}\left(Dn\frac{\partial s}{\partial y}\right) + \frac{\partial}{\partial z}\left(Dn\frac{\partial s}{\partial z}\right) \qquad (4)$$

Mass balance:

$$\frac{\partial}{\partial x}\rho u + \frac{\partial}{\partial y}\rho v + \frac{\partial}{\partial z}\rho w = 0 \qquad (5)$$

Equation of state:

$$\rho = \rho_0(1 + \alpha s) \qquad (6)$$

Where u, v, w are Darcy velocities, p pressure, s salinity (in %, by weight), K_x, K_y, K_z conductivities, D hydraulic dispersion coefficient, n kinematic porosity, α a coefficient $(= 8 \times 10^{-3})$, ρ_0 a reference density of water (= 1 000 kg/m^3), ρ density of water and g gravitational acceleration. The coordinate system is denoted x, y, z with x in the east direction, y north and z vertical upwards.

It is still unclear (at least to the author) how the hydraulic dispersion coefficient ought to be interpreted and determined in a fractured rock. For a general porous media, where a representative elementary volume can be defined, general tensor expressions are available, see Bear et al (1987). A further complicating factor is that we are going to apply the salinity equation in a discretized form, i.e. on our computational grid. A suggestion is that the dispersion coefficient should account for sub-grid mixing processes. Due to the uncertainty about the interpretation of the process we will assume that the dispersion coefficient is isotropic, proportional to the local velocity and the grid-size, hence:

$$D = \beta \Delta |\vec{U}| \qquad (7)$$

where β is an unknown coefficient, Δ the grid-spacing and $|\vec{U}|$ the magnitude of the pore-velocity. As seen, the effect of molecular diffusion is also neglected in (7). As D is multiplied with n in equation (4) we will further assume that n $|\vec{U}|$ is equal to the magnitude of the Darcy velocity. A constant value of 2 metres was set for the product $\beta \Delta$. The sensitivity to this value will be evaluated later in the report.

The suggestion that dispersion should be regarded as a subgrid process in the numerical model is related to the conductivity field used. A stochastically generated field will be used, which means that large scale (i.e. larger than the grid-scale) dispersion will be accounted for by the velocity field. The basic steps in the generation of the conductivity field used by the model are as follows:

- Generate a conductivity for each computational cell using the geometric mean values and standard deviations given in Table 2-1.

- Generate cell-wall conductivities by calculating a geometric mean between the cell and its neighbour. This is done for all cell-walls and hence give a locally anisotropic conductivity, i.e. for a given cell all cell-wall conductivities are different.

- Calculate the length of the fracture zone crossings for each cell-wall. Modify the cell-wall conductivity with respect to the transmissivity of the fracture zones.

Further details can be found in Appendix B.

A method to predict the depth of the unsaturated zone was introduced in Svensson (1995). Here a brief account of the basic idea of the method will be given.

- Neglect capillary forces, which means that the pressure in the unsaturated zone will be equal to the atmospheric pressure (set to zero).

- The unsaturated zone is partly blocked by air and hence provide higher resistance to flow. Introduce a resistance factor, ϕ, in the balance of forces. The vertical balance, equation (3), then reads:

$$0 = -\frac{\partial p}{\partial z} - \frac{\rho g}{K_z} w\phi - \rho g \qquad (8)$$

- For $\phi = 1$ a negative pressure is predicted for the unsaturated zone. The problem is to find a ϕ - field that gives zero pressure in the unsaturated zone and, of course, has a value of 1.0 in the saturated zone. This can be achieved by an iterative procedure, see Svensson (1995) for details and applications.

The system of equations is solved by the general equation solver PHOENICS, Spalding (1981). PHOENICS is based on a finite-volume formulation of the basic equations and embodies a wide range of coordinate systems (cartesian, body-fitted, cylindrical, etc.) and numerical techniques (higher order schemes, solvers, etc.).

4 RESULTS

4.1 DETAILS OF THE MODEL SET-UP

The computational domain is $10 \times 10 \times 3 \, \text{km}^3$, which is represented in a grid with a total of 360 000 cells $(100 \times 100 \times 36)$. Part of the grid is shown in Figure 4-1. As can be seen the grid follows the topography (boundary-fitted grid), but has a uniform cellsize (= 100 metres) in the horizontal plane. The vertically non-uniform grid is restricted to the top 100 metres of the domain. For this part of the grid we start with a cellsize distribution (from groundlevel downwards) as follows: 1, 2, 4, 8, 15, 25 and 45 metres. This sequence of cells is then stretched/compressed to follow the topography, which means that the cell-sizes in the sequence are somewhat smaller below the Baltic and somewhat larger below land. Below 100 metres the cellsize is 100 metres in all three directions. It should be noted that the grid follows the sea-bed and not the free surface of the Baltic.

Conductivities for the top four cell layers, i.e. down to 15 metres, are given a special interpretation. One reason for this is that the soil cover can be expected to have a conductivity which is high, but rapidly decreasing with depth. Another is that small ephemeral rills and channels need to be accounted for by the conductivity of the near ground surface cells. The two major rivers in the domain, Mistraån and Laxemarån, are however accounted for by marking the relevant surface cells and give these a significantly higher conductivity. The flow in the rivers is about 0.1 m^3/s and the cross area of the surface cell is 1 x 100 m^2. Using these data it can be shown that putting the conductivity in the "river cells" to 1.0 m/s gives a hydraulic gradient of 10^{-3}, which seems reasonable. The conductivity of the marked river cells is thus put to 1.0 m/s, while the conductivities of the top four cell layers are considered as calibration parameters. Conductivities below the top four layers are generated with the procedure outlined above. It should be noted that most of the results to be presented are based on one realisation of the stochastic field. The sensitivity to the stochastic conductivity field will however be evaluated and it will be shown that the main results are not sensitive to different realisations.

The fracture zone model was introduced in Figure 2-1. These are the fracture zones considered to be important for the regional scale.
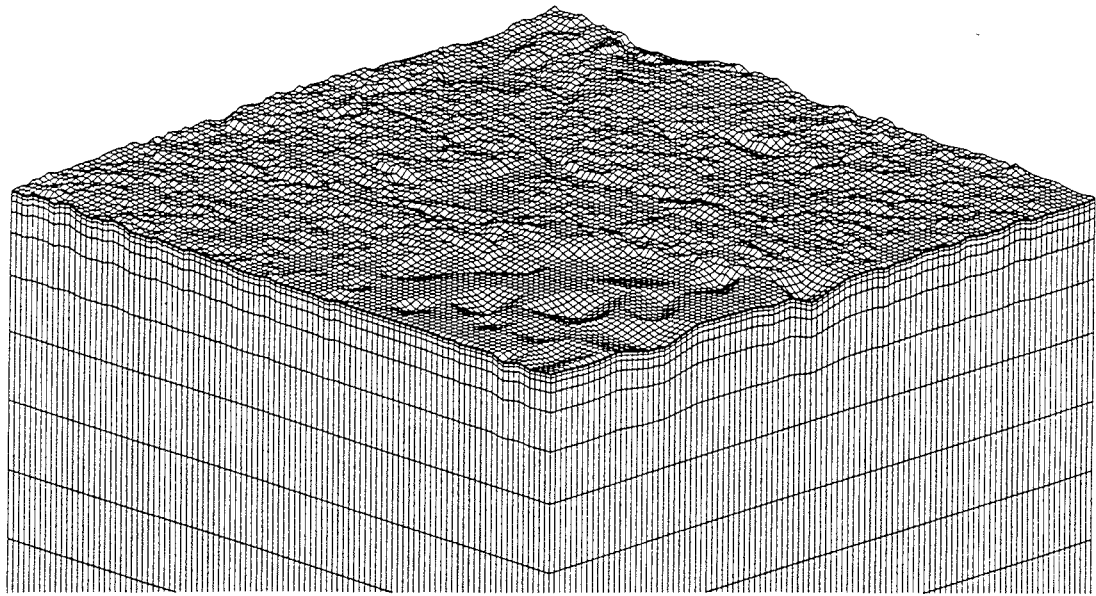
Figure 4-1. *Computational grid close to ground. 100 metres below sea level a uniform grid is used. The vertical scale has been stretched in the figure. View from south-east.*

In one of the cases to be studied the Äspö HRL will be included in the model. This is done by specifying the measured inflows to the tunnel, in the crossings between the tunnel and fracture zones. All local fracture zones on Äspö are however not represented in the fracture zone model for the regional scale. In order to be able to specify the inflows to the tunnel the fracture zones NE3 ($T = 2.9 \times 10^{-4}$ m^2/s) and NE4 ($T = 3.0 \times 10^{-5}$ m^2/s) are included. For details about these fracture zones, see Rhén et al (1997). A fracture zone crossing the spiral part of the tunnel is also needed. A fracture zone, called NNW* (representing all NNW-structures crossing the spiral part of the tunnel), is therefore introduced in order to be able to prescribe the measured inflows to the spiral part of the tunnel. NNW* is vertical, centred through the spiral, has a North-NorthWest orientation, extends from NE1 to EW1 and given a transmissivity of 1.0×10^{-4} m^2/s. With the introduction of NE3, NE4 and NNW* it is possible to distribute the measured inflow to the tunnel to fracture zones as given in Table 4-1 The total measured inflow to the tunnel is about 29.5 l/s (December (1995)).

Table 4-1. Prescribed inflows to Äspö HRL.

Depth (m)	Fracture zone	Inflow (l/s)
→ 120	NE3, NE4	7.5
120-200	NE1	10.0
200-300	NNW*	4.0
300-400	NNW*	6.0
400-500	NNW*	2.0

The "extra" fracture zones introduced are included in all simulations to be discussed. This means that the fracture zone model specified by Rhén et al (1997) has been slightly modified. However, as the fracture zones have a small extension in the regional scale it is expected that the fracture zones only affect conditions locally.

Boundary conditions are set as given pressure (hydrostatic) and salinity distributions at the boundaries facing the Baltic (eastern and part of the southern boundary, see Figure 1-1), while zero flux conditions are assumed for the other vertical boundaries, as well as the bottom boundary. The salinity distribution at the Baltic boundary is set according to the measured distributions at Äspö and Laxemar, see Rhén et al (1997) for details. The following relations are used:

$$s_1(z) = 0.60 + 0.0017 \times Depth$$

$$s_2(z) = -11.42 + 0.0121 \times Depth$$

$$s(z) = \text{MAX}\left(s_1(z), s_2(z)\right)$$

where $s(z)$ is the salinity, in %, specified. *Depth*, is the depth below mean sea level. At the top boundary a net recharge of 200 mm/year is specified above sea level. Below the Baltic Sea a hydrostatic pressure is prescribed, with respect to the local water depth, and the salinity is fixed to the salinity of the Baltic (= 0.6%).

4.2 MODEL CALIBRATION

A groundwater model is normally calibrated by adjusting conductivities and transmissivities to meet some predefined conditions, for example the drawdown due to a pumptest. For the calibration of the present regional model, only a limited set of data is available. These data mainly concern near-ground conditions and we will therefore choose to calibrate the model with the conductivities of the top four layers. The chosen calibration criteria are:

- The model should simulate measured groundwater levels on Laxemar and Ävrö under natural conditions, i.e. the Äspö HRL is not present.

- The model should simulate "wet areas" (lakes, peat areas, etc.) as given by maps of the area.

- The calculated flow rates in Mistraån and Laxemarån should be of the right magnitude.

- The maximum groundwater level on Äspö, for natural conditions, should be correctly simulated.

- With the Äspö HRL present the maximum drawdown above the spiral should be of the right magnitude.

- The vertical salinity distributions, as given by measurements in boreholes, on Laxemar and Äspö should be reproduced.

A trial and error strategy was used to obtain a set of conductivities that meet the criteria in an acceptable way. The final set of conductivities for the top four cell layers was (from ground downwards) 2.0×10^{-3}, 8.0×10^{-4}, 5.0×10^{-6} and 1.0×10^{-6} m/s. These conductivities are applied horizontally uniformly, which means that we have the same conductivity set below the Baltic Sea as on land.

Measured and predicted groundwater levels on Laxemar and Ävrö can be found in Table 4-2. The location of the boreholes is given in Figure 4-2. The measured groundwater levels are from 1989 and 1990 and thus represent natural conditions. At a first glance the bad agreement in a point by point comparison may be disturbing. However, one should remember that the model has a horizontal resolution of 100 metres and "sub-grid" topographical features are likely to influence the measured values. We can thus not expect more than an agreement for the averaged values.

In Figure 4-3 the "wet areas" and the flow in these are shown. The areas have been marked as wet if the groundwater table is closer than 0.5 m to ground. When comparing the marked areas in Figure 4-3 with the general hydrology of the area, given in Figure 1-1, one should remember that small rills and channels will be represented as saturated areas in the model. The two major rivers are predicted to have a flow rate of about 0.1 m³/s (Mistraån) and 0.05 m³/s (Laxemarån). According to Rhén et al (1997) the estimated runoff for the area is 0.006 m³/(s, km²). From this the catchment areas (in the model) should be 16 km² for Mistraån and 8 km² for Laxemarån, which fits quite well.

Next the conditions on Äspö are studied. With the goal to have the correct maximum groundwater level, which is about 5 metres, for natural conditions and a realistic drawdown with Äspö HRL present, it was found that a local calibration for Äspö was required. The local calibration involved a rectangle (1.4 x 1.2 km^2) oriented in the Äspö coordinate system and just enclosing Äspö. It was found that the conductivity of the top four layers should be multiplied with 0.3 and the rest with 0.5. This is actually in line with Rhén et al (1997), who give slightly lower conductivities for Äspö than those given in Table 2-1. The maximum groundwater level for natural conditions was calculated to be about 5 metres. The calculated drawdown with the Äspö HRL present (detailed results will be presented later in the report) was about 60 metres, which is less than the real drawdown. However, considering the resolution in the model, it was concluded that the drawdown in a 100 x 100 metres cell ought to be in the range 50-70 metres.

Finally, the calculated vertical distributions of salinity are compared with measured distributions, see Figure 4-4. The most important information in this figure is that the freshwater lens below Äspö is about 250 metres, while the two boreholes on Laxemar give 700 and 900 metres. The model is found to reproduce these values quite well.

The conclusion from this calibration exercise is that the calibrated model is in fair agreement with the limited data available. This has been achieved by specifying the conductivity of the top four layers of cells, a local calibration on Äspö and by introducing three local fracture zones crossing the Äspö HRL.

Table 4-2. Calibration of groundwater table. Comparison between measured and predicted levels (metres above sea level) for Laxemar and Ävrö after calibration.

Borehole	Measured level (m)	Predicted level (m)
Laxemar		
hlxo1	6.7	11.6
hlx02	4.8	1.7
hlx03	5.4	6.9
hlx04	8.1	8.4
hlx05	14.2	7.1
hlx06	9.0	11.8
hlx07	6.20	6.9
klx01	9.4	8.9
Average	7.97	7.91
Ävrö		
hav01	1.6	3.2
hav02	1.4	0.3
hav03	0.5	0.1
hav04	4.5	4.5
hav05	2.8	0.1
hav06	5.3	6.3
hav07	0.9	2.3
hav08	0.5	1.5
kav01	8.2	4.4
kav02	2.9	2.2
kav03	0.2	0.1
Average	2.62	2.27
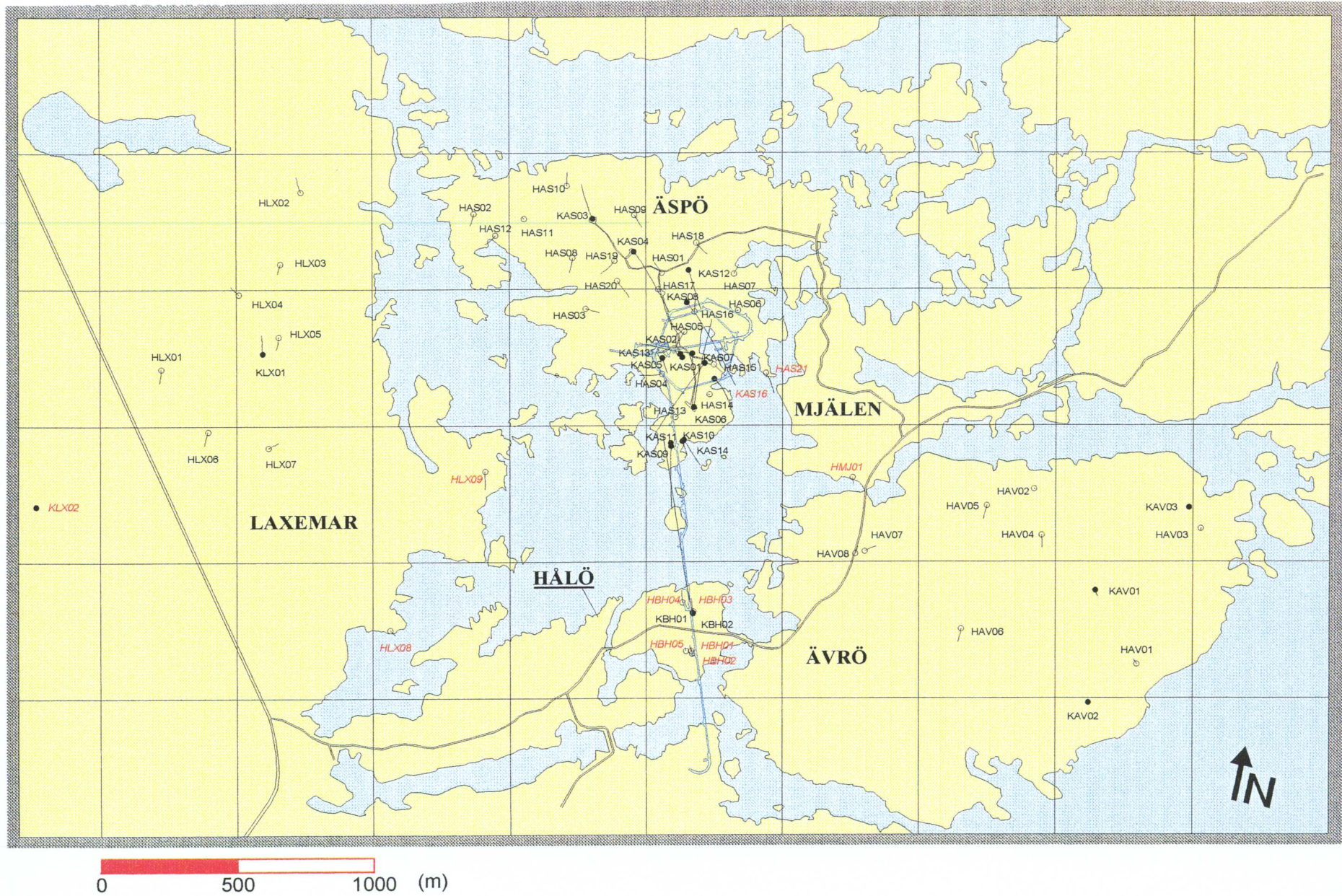
Figure 4-2. Boreholes on Laxemar, Ävrö and Äspö.
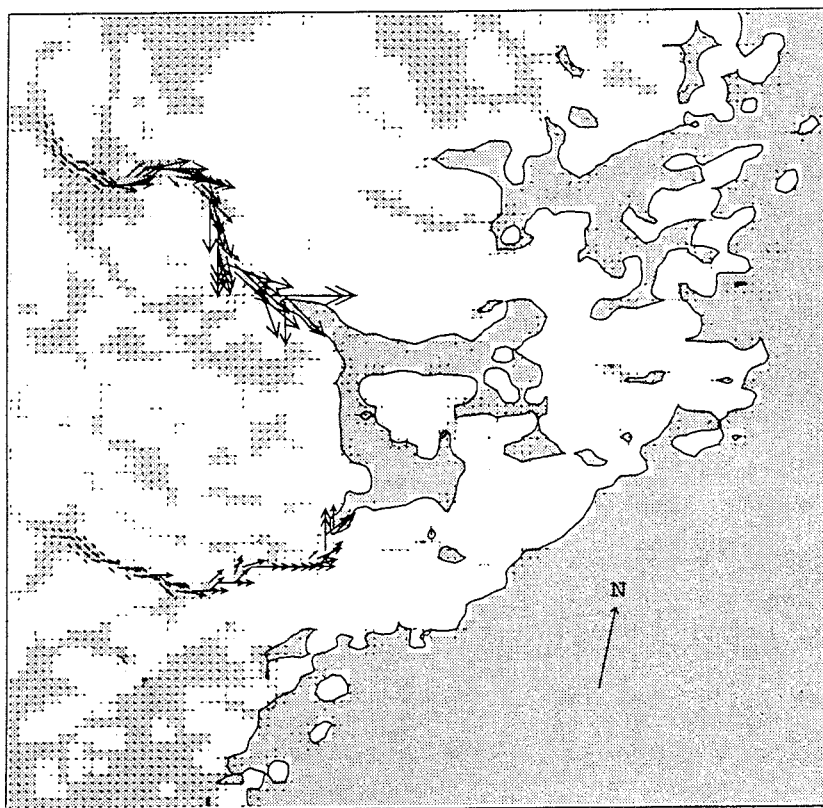
Scale: |-----| 1000 m

Figure 4-3. Flow and saturated areas at ground level. Areas with a
groundwater table less than 0.5 m from ground level have been
marked as saturated areas (shaded in the figure).
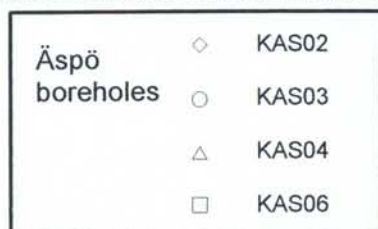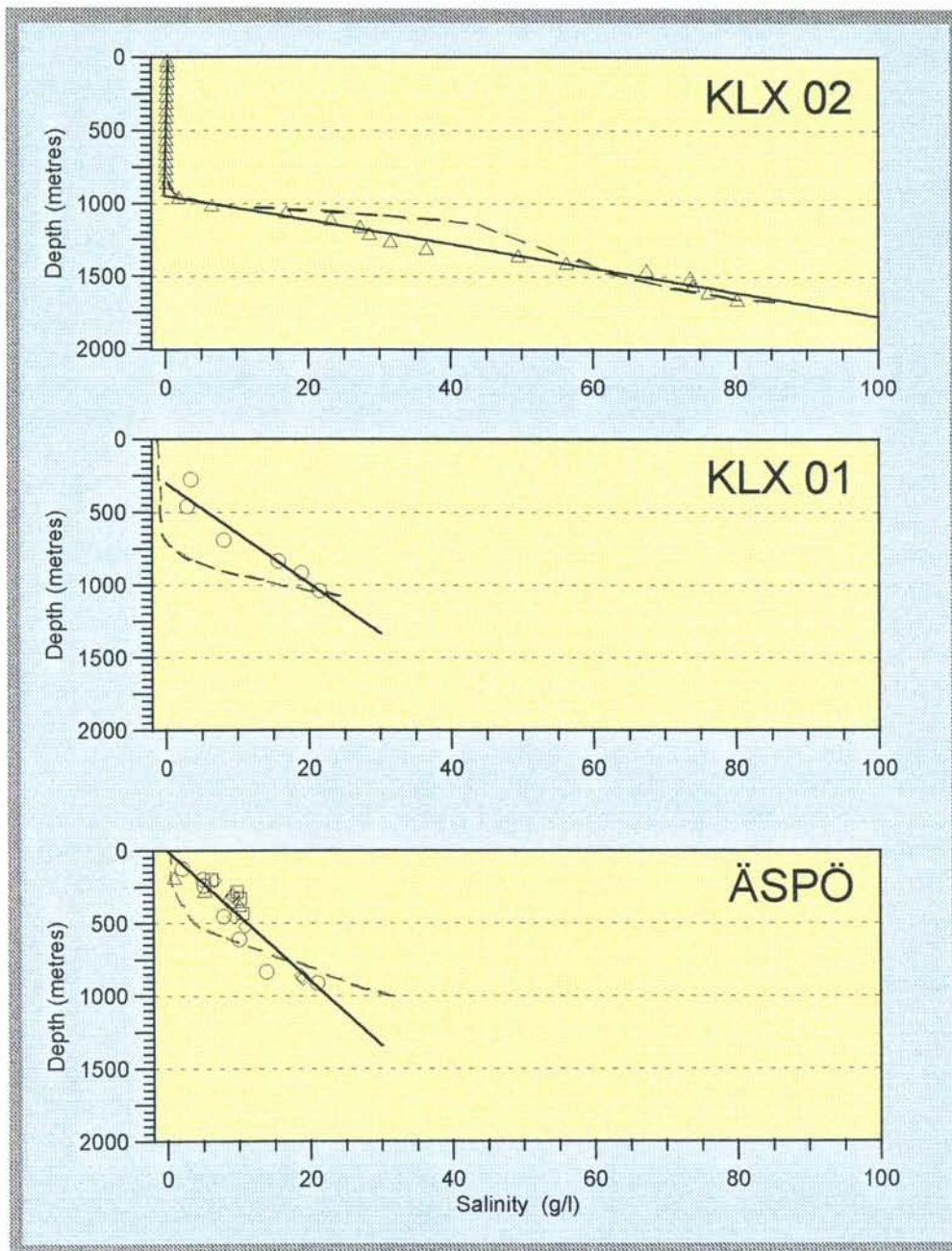Darcy velocity scale : ———▸ 10^{-3} m/s.

Figure 4-4. Measured and simulated (----) vertical salinity profiles on Äspö and Laxemar (KLX01, KLX02). Basic figure from Rhén et al (1997).

4.3 NATURAL CONDITIONS

Some results for natural conditions were presented in the previous section. These will in this section be complemented with more detailed descriptions.

The assigned hydraulic conductivity field, including the fracture zones and the stochastically generated rockblock conductivity, is illustrated in Figure 4-5. As most of the fracture zones are vertical, the vertical conductivity was used for the figures. An examination of the conductivity field shows that the fracture zones marked "W" (less water bearing) in Figure 2-1 do not contribute significantly to the conductivity interval plotted. The zones marked "WW", NE3 and NE4 can however be identified. The lower value in the conductivity interval represents a level where the rockblock conductivity starts to be significant, as can be understood from the figure.

The calculated groundwater table is shown in Figure 4-6, together with the topography as represented in the model. As can be seen, the maximum ground water level is about 22 metres above sea level.

Further insight into the groundwater recharge and runoff can be gained from Figures 4-7, 4-8, 4-9 and 4-10. In Figures 4-7 and 4-8 the horizontal flow at four depths are shown. Two metres below ground large areas are unsaturated (only vertical flow), while at five metres most areas contribute to the horizontal flow. At 250 and 450 metres depth the picture is somewhat different; the flow now reflects the fracture zone system and the stochastic background conductivity. When studying Figures 4-7 and 4-8 one should note the very different scales used for plotting the vectors. Figures 4-9 and 4-10 give the vertical flow distribution at various depths. Also in these figures one should note the various isoline values used to illustrate the flow. The general vertical flow pattern is downwards in high areas and upwards in low areas, below rivers and along the coast. At 500 metres depth we still find this pattern which may seem surprising. This is however due to the density distribution as will be explained by the vertical sections to be discussed next.

Two vertical sections through the Äspö HRL are shown in Figure 4-11. The isolines for salinity indicate that the fresh water lens below Äspö is about 200 metres deep, while the fresh water in the Laxemar area penetrates down to about 700-800 metres. This explains why the flow at 400-500 metres depth, see figures above, is stronger below Laxemar; below Äspö we have a stable stratification and almost stagnant conditions at this depth.
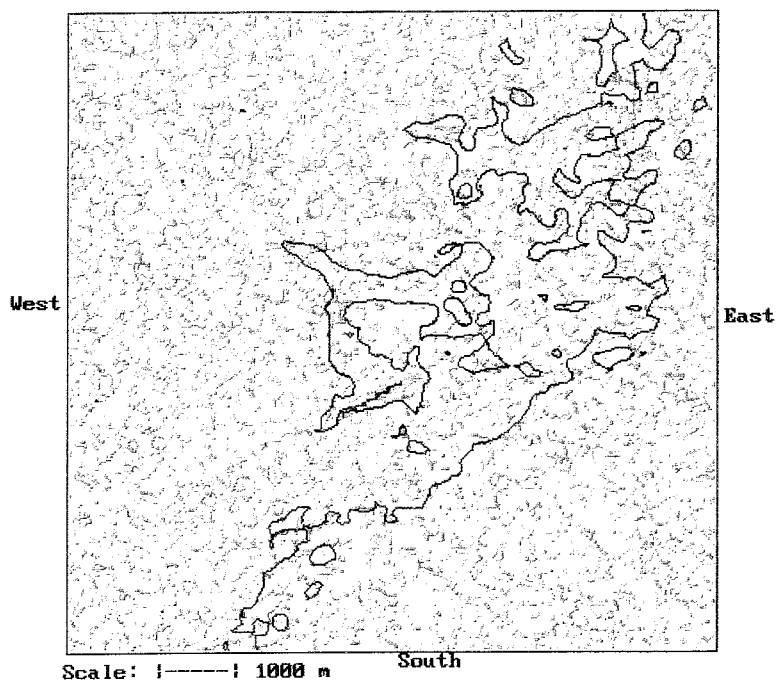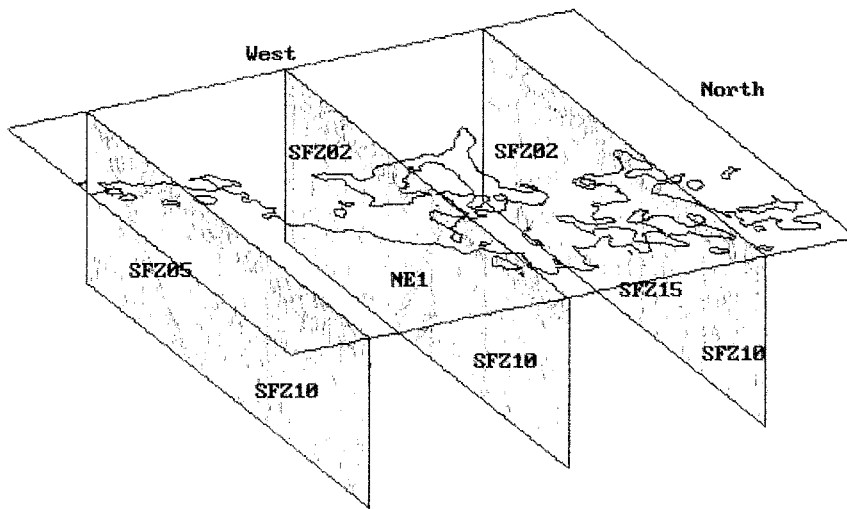
Figure 4-5. Illustration of conductivity field. Perspective view (top) and horizontal section at a depth of 450 metres. Plotted conductivity interval: $2.5 \times 10^{-7} \rightarrow 5.0 \times 10^{-5}$ m/s.

TOPOGRAPHY
[M]
-31
-27
-23
-19
-15
-11
-7
-3
2
6
10
14
18
22
26

Scale: !------! 1000 m

GR.W.LEVEL
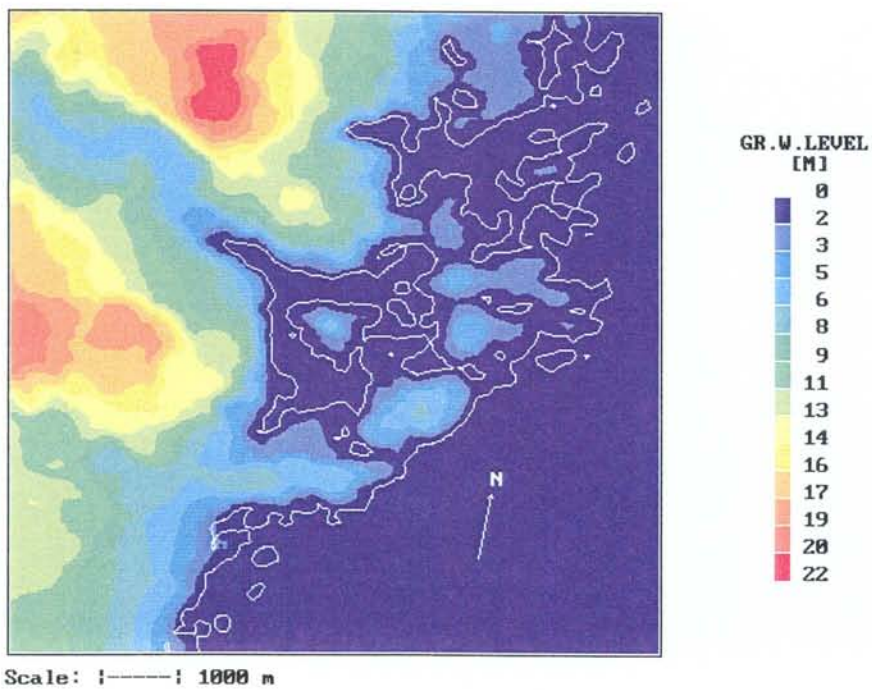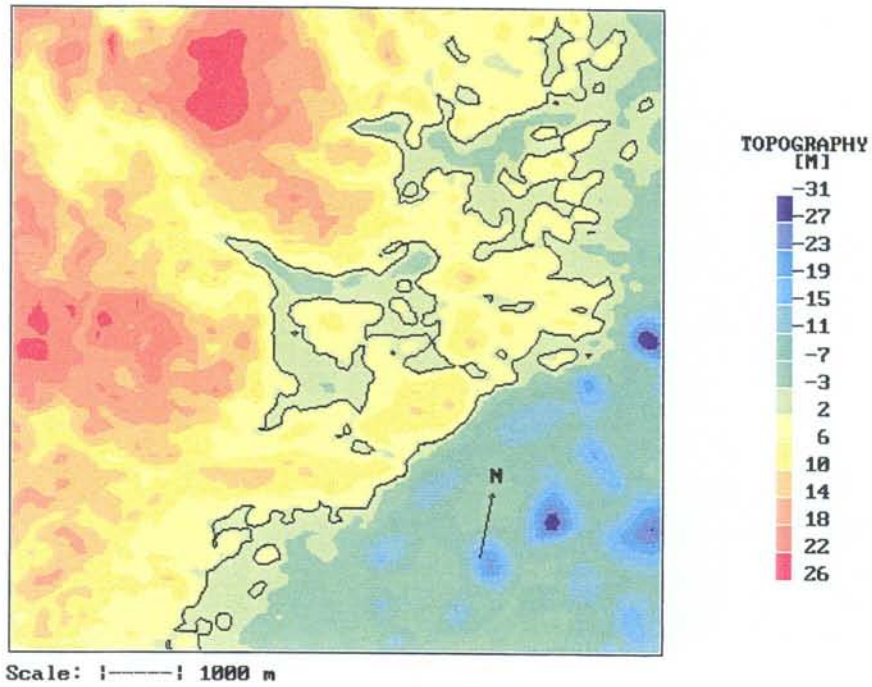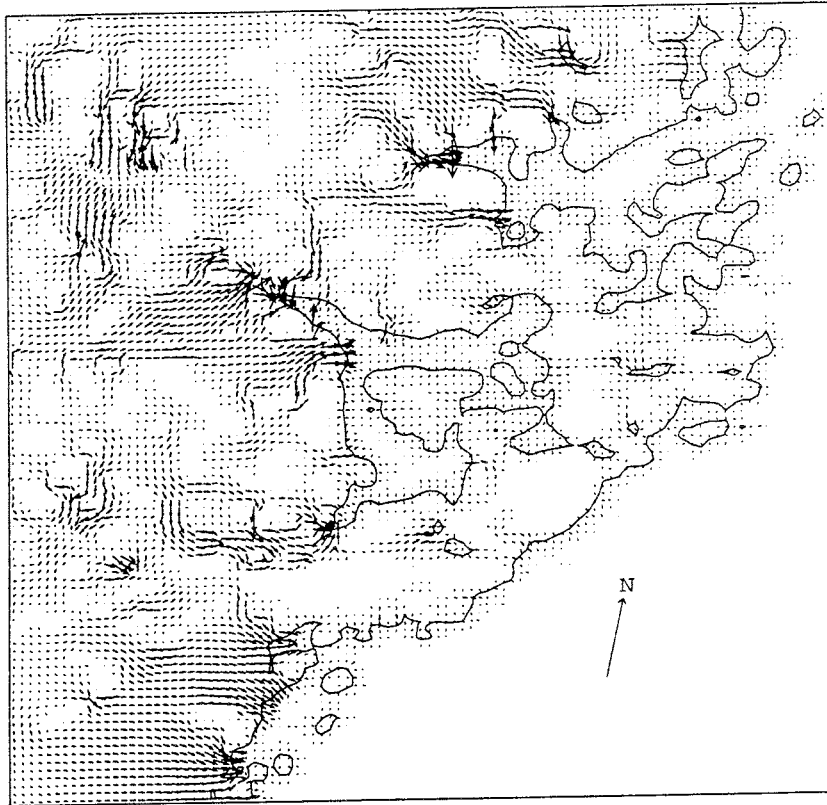[M]
0
2
3
5
6
8
9
11
13
14
16
17
19
20
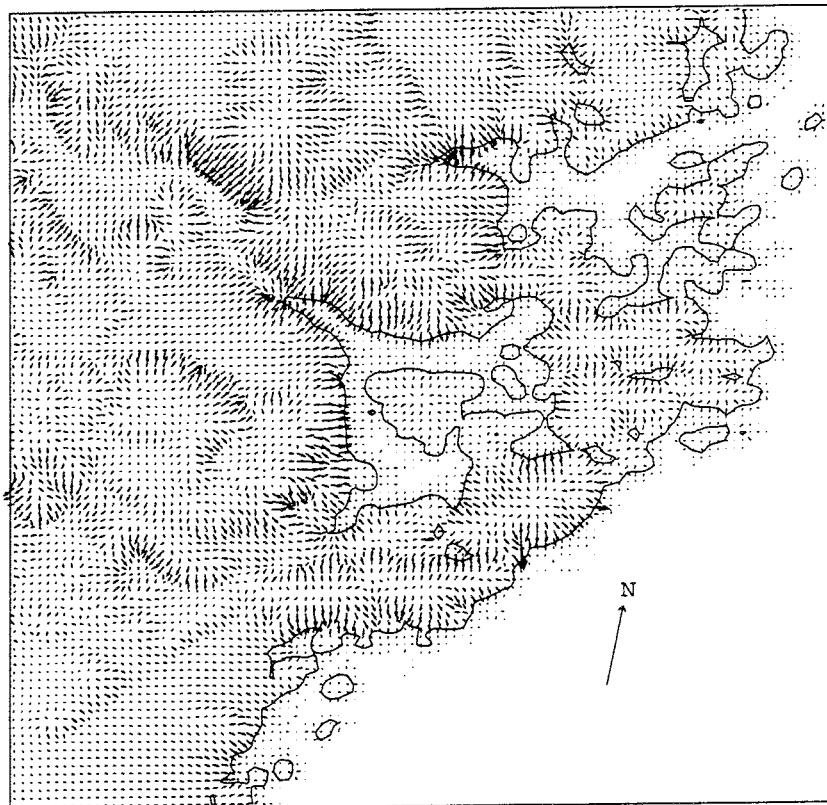22

Scale: !------! 1000 m

Figure 4-6. Topography (top) and predicted groundwater table (metre above sea level) for natural conditions.
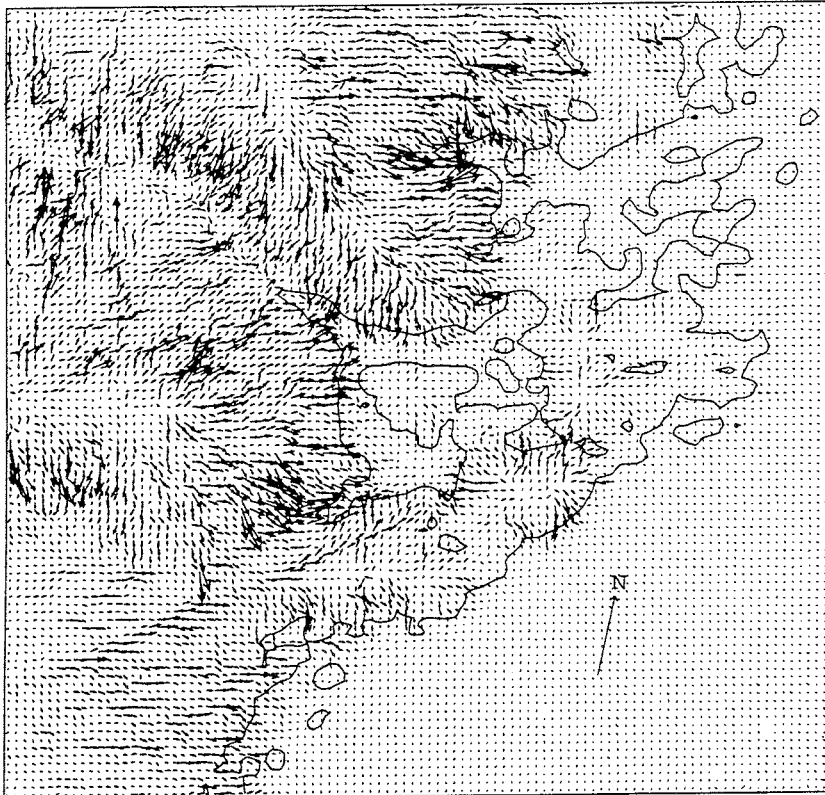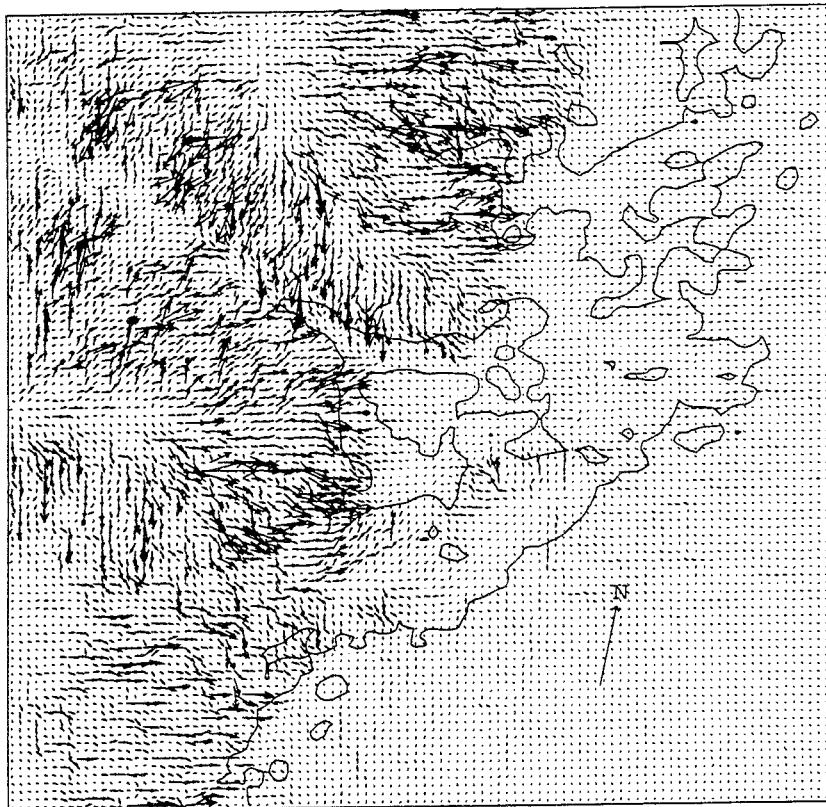
20

Scale: |-----| 1000 m

Scale: |-----| 1000 m

Figure 4-7. Horizontal flow at two metres (top) and five metres depth. Natural conditions.

Darcy velocity scale: ⟶ $5 \times^{-5}$ m/s (top)

⟶ 1×10^{-6} m/s (bottom)

Scale: |-----| 1000 m

Scale: |-----| 1000 m

Figure 4-8. Horizontal flow at 250 metres (top) and at 450 metres depth. Natural conditions.
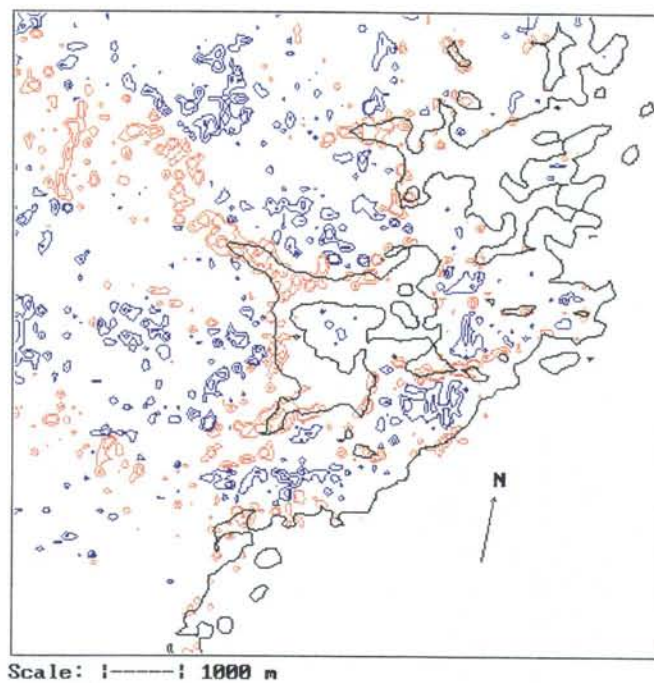
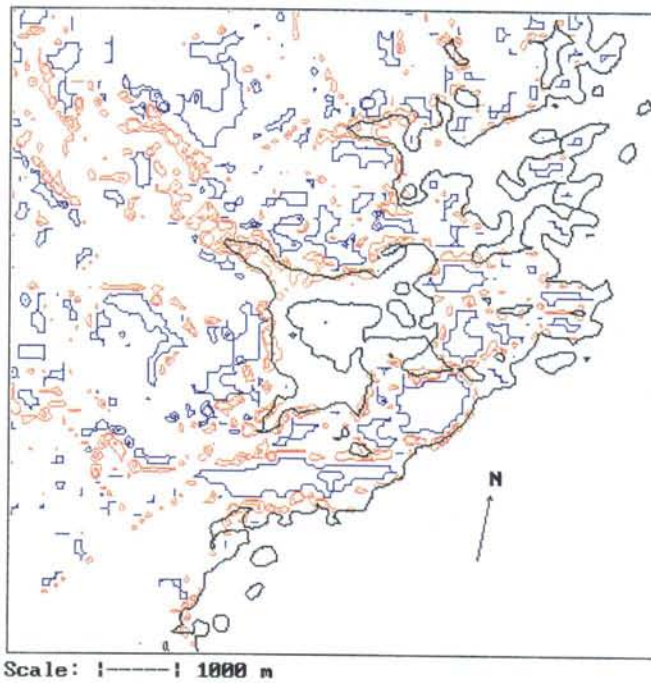Darcy velocity scale: ———→ 2×10^{-8} m/s.

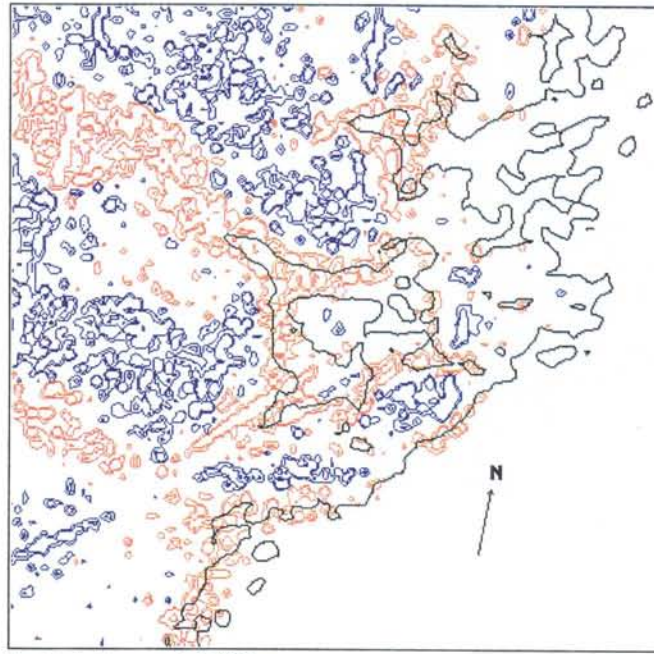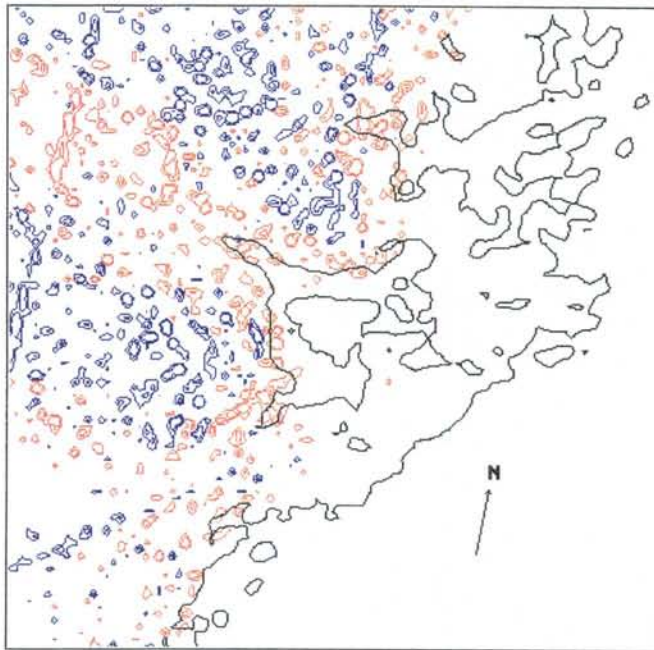*Figure 4-9.* Vertical flow at 3.0 (top) and 30.0 metres depth.
Blue colour indicates downwards and red upwards flow. Natural
conditions.
Isoline values: 200 and 400 mm/year (top)
                100 and 200 mm/year (bottom).

23

Figure 4-10. *Vertical flow at 200 metres (top) and at 500 metres depth. Natural conditions.*
Blue colour indicates downwards and red upwards flow. Isoline values: 20 and 40 mm/year.

24

South   Äspö   North

Scale: |------| 1000 m

West   Äspö   East
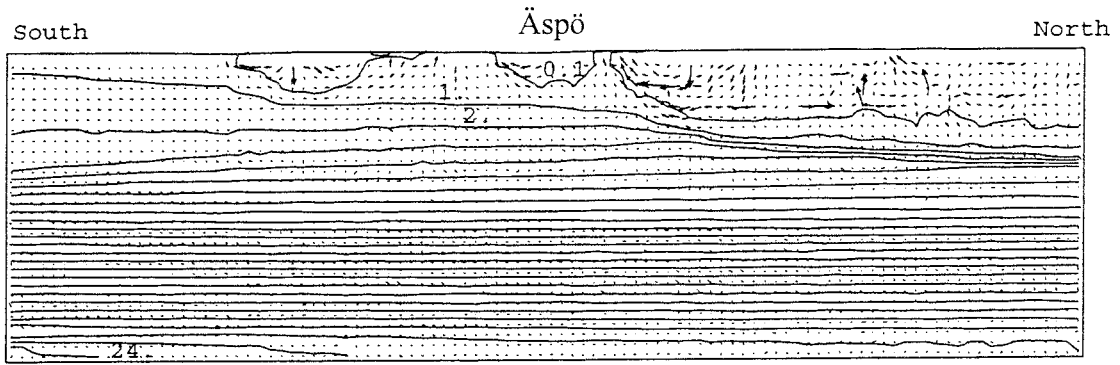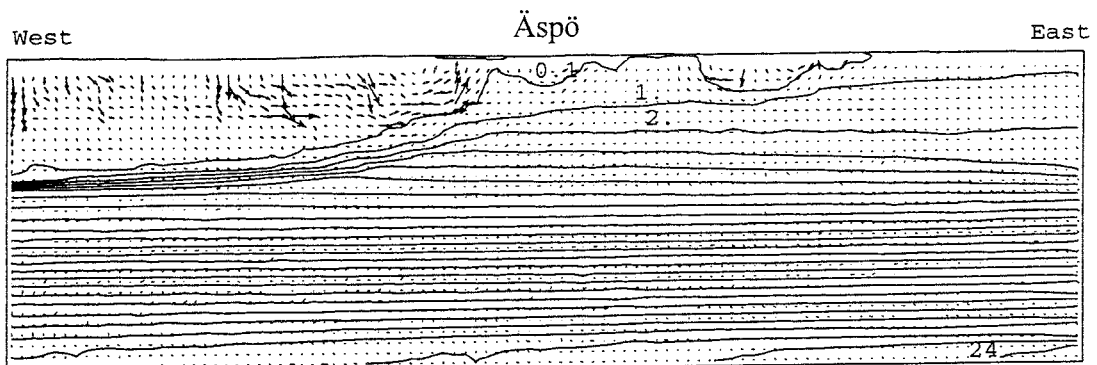
Scale: |------| 1000 m

Figure 4-11. North-South (top) and East-West vertical sections through Äspö HRL. Flow and salinity fields (in %). Natural conditions.

Darcy velocity scale : ———→ $2 \times 10^{-8} m/s$

(Note: flow from ground to 100 metres depth not shown).

4.4 WITH ÄSPÖ HRL PRESENT

The main influence on the flow, pressure and salinity distributions from the Äspö HRL is through the inflows to the tunnel. These inflows are concentrated to tunnel sections with fracture zone crossings. The fracture zones crossing the tunnel and the inflow distribution were given earlier, see Table 4-1.

The groundwater table and the near-ground vertical flow, with the Äspö HRL present, are shown in Figure 4-12. The drawdown above the tunnel is seen to be predicted to 60 metres, this is a value that was regarded as realistic (considering the 100 metres discretization scale) in the local calibration procedure described above. A groundwater level of 3-4 metres above sea level is found on the northern part of Äspö.

The vertical flow at 3 metres depth is similar to that for natural conditions, except for Äspö and south of Äspö. Here the vertical flow is predicted to be above 400 mm/year.

The horizontal flow pattern at 250 and 450 metres depth is found in Figure 4-13. This figure should be compared with Figure 4-8, where the same situation without the tunnel is shown. It is interesting to note that the influence of the tunnel is restricted to a radius of 500-1 000 metres.

Two vertical sections, to be compared with Figure 4-11, are shown in Figure 4-14. As seen the tunnel will influence the salinity distribution down to 1 500 metres and also influence the near ground distribution, as given by the 0.1% isoline, significantly. Looking at the E-W section one may even expect fresh water from the Laxemar area to end up in the tunnel.
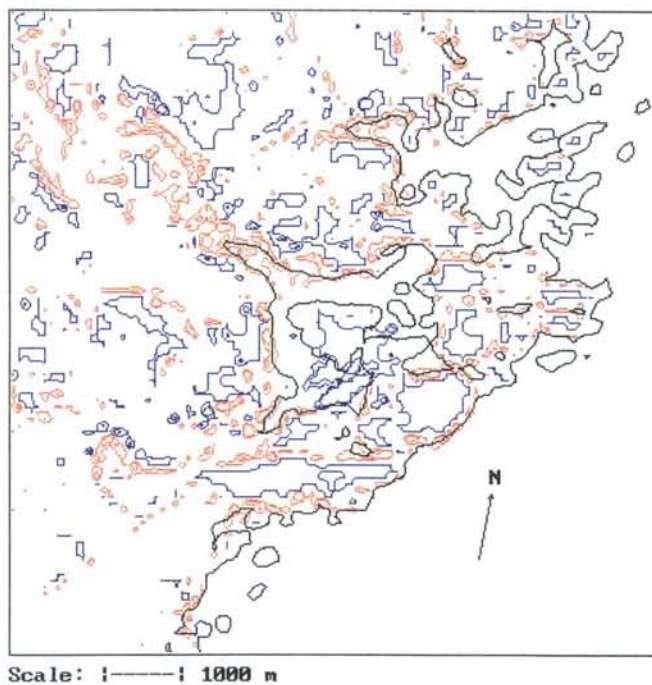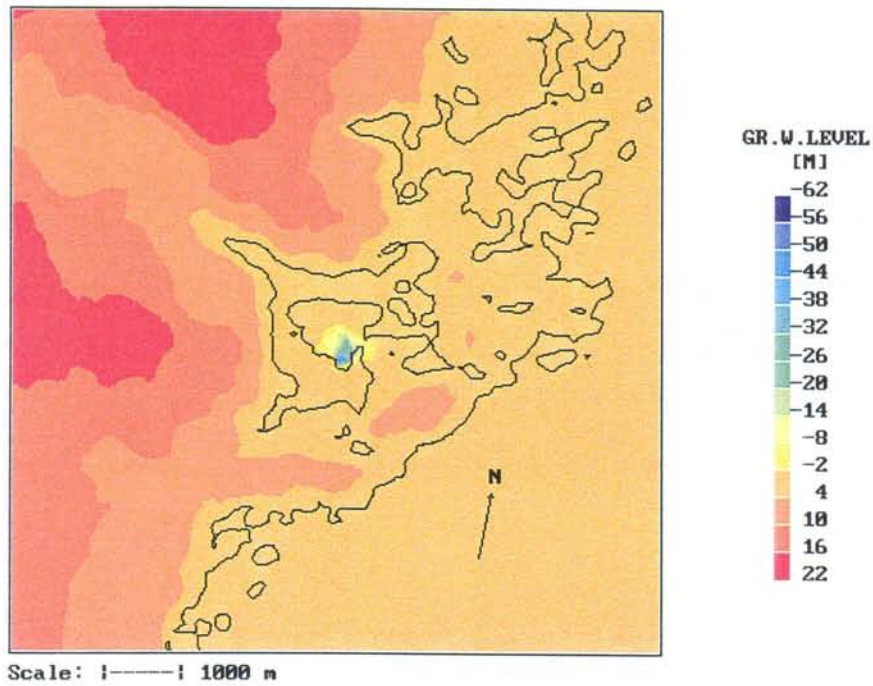
Figure 4-12. *Groundwater table (metres above sea level) (top) and vertical flow at 3 metres depth with Äspö HRL present. For vertical flow blue colour indicates downwards and red upwards flow. Isoline values: 200 and 400 mm/year.*

27
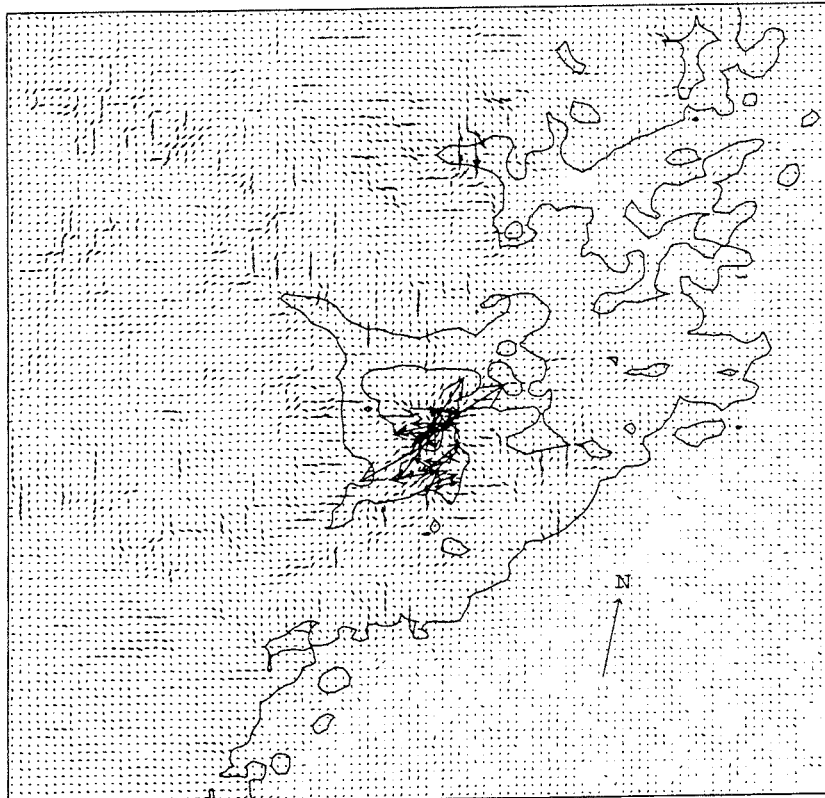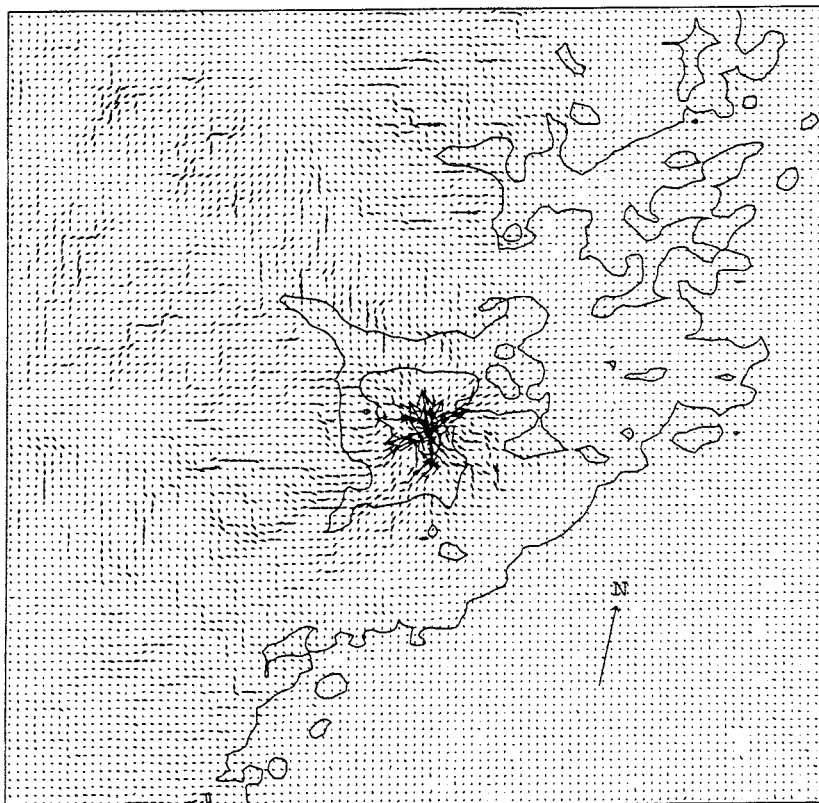
Scale: |-----| 1000 m

Scale: |-----| 1000 m

Figure 4-13. Horizontal flow at 250 (top) and 450 metres depth with Äspö HRL present.

Darcy velocity scale: $\longrightarrow$ 5×10^{-8} m/s.

South   Äspö   North

Scale: |------| 1000 m

West   Äspö   East

Scale: |------| 1000 m
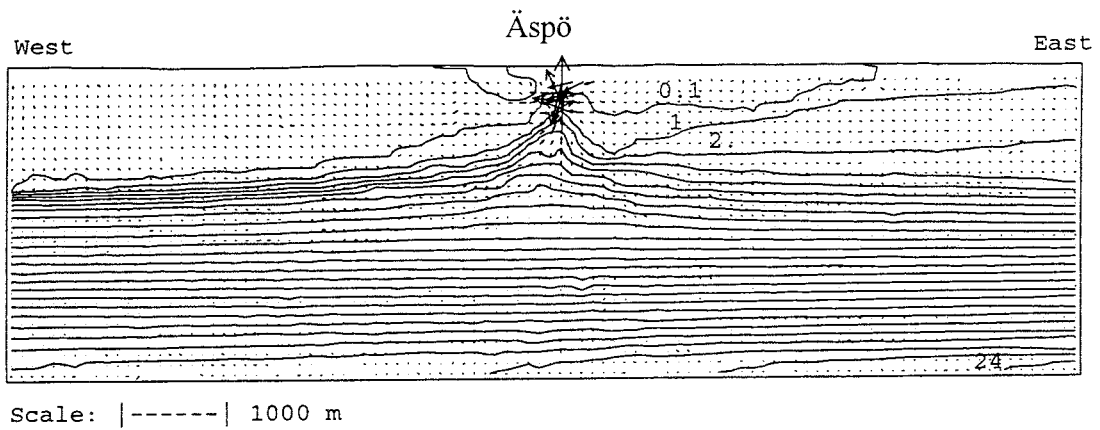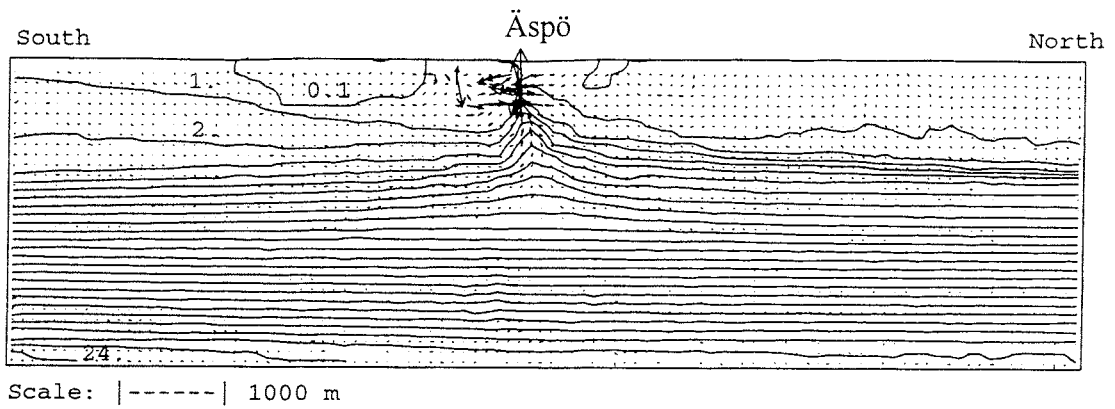
Figure 4-14. *North-South (top) and East-West vertical section through Äspö HRL, with tunnel inflow present. Flow and salinity (in %) fields.*
Darcy velocity scale: ⟶ 2×10^{-7} *m/s.*
(Note, flow from ground to 100 metres depth not shown).

4.5 BOUNDARY CONDITIONS FOR A SITE MODEL

One of the purposes of the present study is to establish relevant
boundary conditions for a site model. Such data can easily be
extracted from the regional model presented. From a general point
of view it is however also of interest to study "the radius of
influence " for the Äspö HRL. When a site model is set up one
strives to have a domain size large enough for the tunnel not to
influence the boundary conditions.

Predictions intended to shed some light on these questions are
shown in Figures 4-15, 4-16 and 4-17. In these figures the
differences, in pressure and salinity, between natural conditions and
with Äspö HRL present are plotted. Starting with the vertical
sections showing the pressure difference, see Figure 4-15, we see
that the maximum pressure drop is about 50×10^4 Pa (note that the
discretization scale is 100 metres) and that the low pressure spreads
out horizontally at a depth of about 1 500 metres. The response in
the salinity field, see Figure 4-16, is that the fresh water interface is
moved downwards under the high-topography areas West and
North of Äspö. Right below the tunnel the salinity is increased as
salt water from below is drawn towards the tunnel (upconing). The
horizontal pressure drop distribution at 450 metres depth, see
Figure 4-17, shows that the main influence of the tunnel is limited
to a radius of about 1 km. However, as discussed above, the
pressure deficit spreads out laterally at a depth of about 1 500
metres.

The results have a resemblance to a process called selective
withdrawal, well studied in the theory of stratified flows. According
to this principle only water from a certain density range is
withdrawn from a stratified fluid. It is too early to conclude that the
Äspö HRL generates a large scale horizontal flow, in accordance
with the selective withdrawal principle, but the simulations
certainly points to a possible solution, not considered earlier.

When the repository is in operation there will be no inflows to the
tunnel and the situation is back to natural conditions. It is of course
of interest to study the boundary conditions for a site scale model
also for this case. These boundary conditions can be obtained from
the regional model. An integral characterisation of the flow and
transport around a repository can also be achieved by studying
fluxes over the boundaries of a box enclosing the repository site.
This has been done using a box of 2 x 2 km^2 in the horizontal plane
(centred around the Äspö HRL) and extending from -100 to
-1 000 metres below sea level. The reason for having the top
boundary of the box at 100 metres depth is that we want to exclude
the near-ground fluxes as these would dominate the fluxes and
mask the influence of the tunnel. In Table 4-3 the volume and salt

fluxes across the six faces of the box are summarised. It should be noted that the positive coordinate directions are in the east, north and up directions, which means that a positive flux at one of these boundaries is an outgoing flux. For natural conditions we find that the flux is mainly from West (Laxemar) and South and it leaves the box at the top boundary. With the tunnel present all boundaries have an inflow; most of the flux comes however from the top boundary. For each boundary a separation of in- and outgoing fluxes is also given. The values for the West boundary under natural conditions (1.91-0.01) thus mean that 1.91 l/s is flowing into the box and 0.01 l/s is leaving the box. This gives a rough estimate of how uniform the flow is. A similar analysis can be done for the convective salt fluxes across the boundaries, see Table 4-3. For natural conditions we find that the East, West and South boundaries provide the saltwater that leaves at the top boundary. With the tunnel present all boundaries contribute to the salt that enters the tunnel. Using the total inflow of salt and the inflow to the tunnel (29.5 l/s) we obtain an average salinity for the water that enters the tunnel of about 0.5%.

Table 4-3. Volume (l/s) and salt (g/s) flux across the boundaries of a box of 2 x 2 x 0.9 km³ centred around Äspö HRL.

Case	Boundary flux					
	West	East	South	North	Bottom	Top
Natural conditions Volume flux [l/s]	1.90 (1.91-0.01)	-0.38 (0.01-0.39)	0.69 (0.75-0.06)	0.09 (0.13-0.04)	-0.01 (0.13-0.14)	2.87 (3.62-0.75)
With Äspö HRL Volume flux [l/s]	2.93 (2.93-0.00)	-1.67 (0.01-1.68)	1.39 (1.43-0.04)	-1.32 (0.04-1.36)	0.61 (0.68-0.07)	-21.48 (1.04-22.52)
Natural conditions Salt flux [g/s]	1.72	-1.52	1.57	0.14	-0.04	4.50
With Äspö HRL Salt flux [g/s]	3.60	-8.70	4.43	-4.65	32.55	-86.05

Figure 4-15. *North-South (top) and East-West vertical sections through Äspö HRL, showing the pressure difference between natural conditions and with Äspö HRL present.*
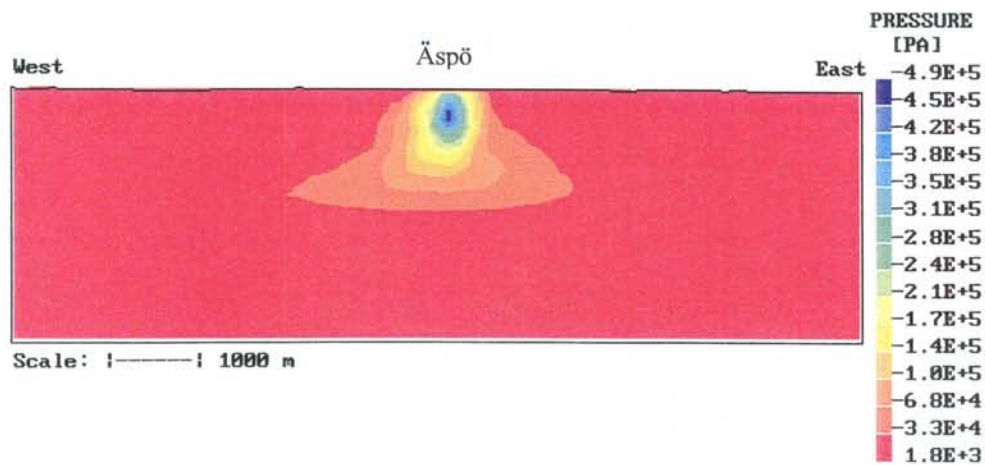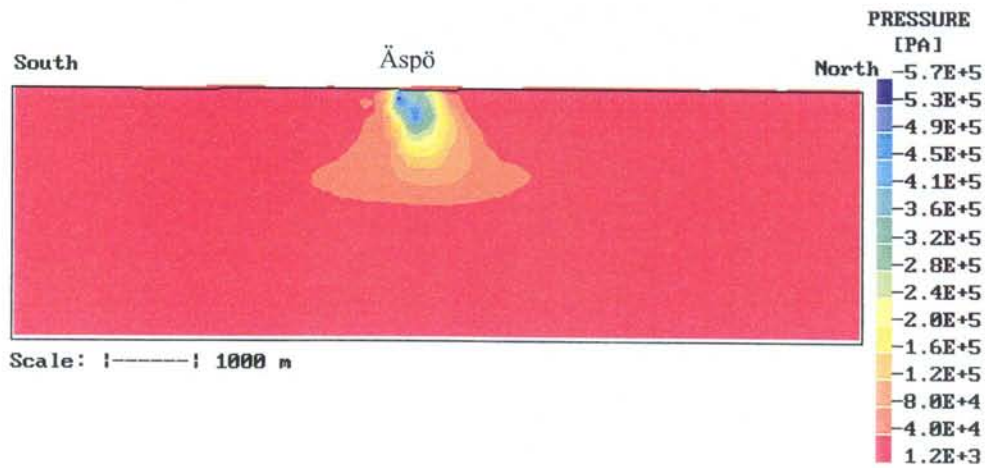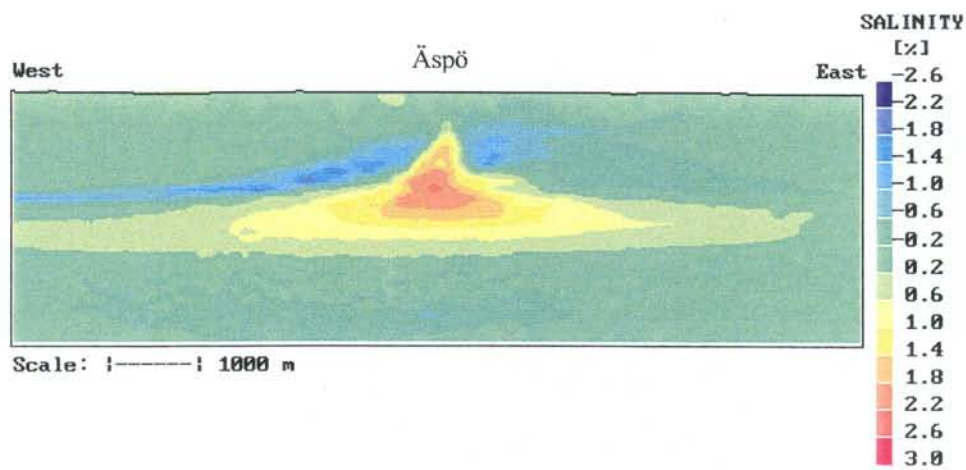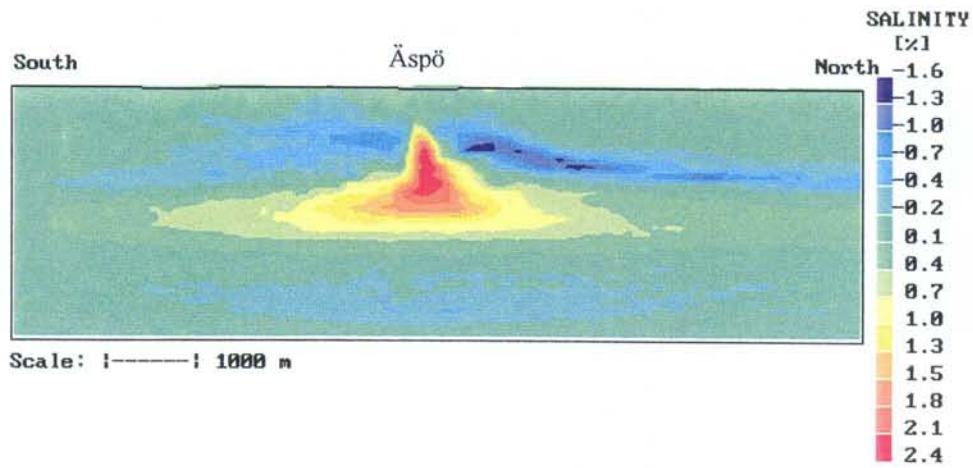
Figure 4-16. North-South (top) and East-West vertical sections through Äspö HRL, showing the salinity difference between natural conditions and with Äspö HRL present.
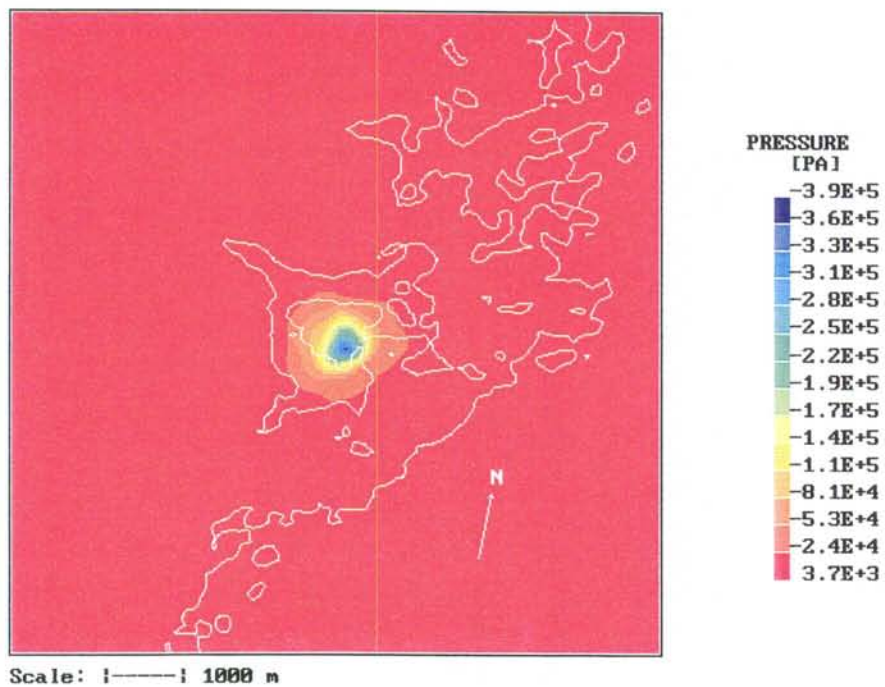
Figure 4-17. *Horizontal section at 450 metres depth showing the pressure difference between natural conditions and with Äspö HRL present.*

4.6 SENSITIVITY TO THE CONDUCTIVITY FIELD

As discussed above, the conductivity fields have two components; a deterministic fracture zone model and a stochastically generated conductivity for the rock mass between the fracture zones. In order to evaluate the sensitivity of the simulations to the conductivity fields one should vary the transmissivities within their estimated uncertainty limits and make several realisations of the stochastic part of the fields. Presently we have no information about uncertainty limits for the transmissivities, and the mean values and standard deviations for the "good rock" are also uncertain. In view of these uncertainties it is expected that the following set of calculations may give an illustration of how sensitive the simulations are to various assumptions regarding the conductivity field.

- Study the sensitivity to alternative realisations of the conductivity field for the rock mass between the fracture zones (hereafter called the background conductivity).

- Assume that there is no vertical variation in mean and standard deviation values for the background conductivity.

- Prescribe a background conductivity field without any stochastic variation, i.e. the standard deviation is zero.

- Study how an anisotropic background conductivity affects the results.

- Increase/decrease the transmissivities with an order of magnitude.

The conductivities and transmissivities given in Chapter 2 constitute our reference case and the above list of calculations thus intend to show how departures from the reference case may affect the simulations.

The first case deals with the sensitivity to alternative realisations of the background conductivity field. Five conductivity fields were generated and these were used for simulations of natural conditions and with the Äspö HRL present. One set of results is shown in Table 4-4, where the variation in groundwater table on Äspö is shown. As can be seen, the drawdown above the Äspö HRL varies significantly (± 20%) for different realisations. In Figure 4-18 the pressure drop and salinity change due to the Äspö HRL are shown along a west to east coordinate, through the centre of the spiral at a depth of 450 metres. Also here five realisations are shown. The centre of the spiral is at coordinate 5 200 metres, as can be

35

understood from the pressure drop curves. From the curves in Figure 4-18, one can conclude that different realisations of the stochastic conductivity field mainly affect the details of a simulation while the gross features are not affected.

Table 4-4. Sensitivity of groundwater table on Äspö to the stochastic conductivity field.

Realisation number	Groundwater level (m)				
	1	2	3	4	5
Maximum groundwater level for natural conditions	4.9	5.4	5.0	5.4	5.1
Minimum groundwater level with Äspö HRL present	-60.	-58.	-67.	-43.	-51.

Next we will make the assumption that the mean background conductivity and its standard deviation have no depth dependence. The mean value was put to 2.0×10^{-7} m/s and the standard deviation to 0.72, based on the values for a depth down to 600 metres as given in Table 2-1. The resulting flow field at 450 metres depth can be studied in Figure 4-19 (top). Initially the idea was to show how the groundwater table was affected by the various assumptions about the conductivity field. The effect was however so small that the flow at 450 metres depth was chosen for this and also the following cases. The flow shown in Figure 4-19 (top) is very close to the reference case, see Figure 4-8. The only difference is that the flow is somewhat higher in the reference case which is explained by the higher conductivity at this depth in the reference case, see Table 2-1.

If the standard deviation is put to zero (all other conditions according to the reference case), the flow shown in Figure 4-19 (bottom) is simulated. It is here clearly illustrated that it is only the fracture zones classified as "water bearing" (marked "WW") in Chapter 2, that show up as distinct features.

In order to study how an anisotropic background conductivity may affect the flow field the conductivities in a NW/SE direction (with North according to the Äspö coordinate system) were increased by an order of magnitude while a decrease with an order of magnitude was applied in the NE/SW direction. The result is shown in Figure 4-20. As can be seen, a totally different flow pattern results.

The final case to be discussed concerns the fracture zones. In order to see the significance of these two simulations were performed; one with all transmissivities increased by an order of magnitude and the other with transmissivities decreased by the same amount.

The result is shown in Figure 4-21. Also in this case significant effects can be found; if the transmissivities are increased the fracture zones will dominate the flow pattern, if they are decreased the influence of the fracture zones disappears.

In order to get some quantitative measures of how the various assumptions about the conductivity field affects the conditions below Äspö the "box analysis" introduced in Section 4.5 will be employed. The flow and salt transport through the box boundaries are given in Table 4-5 for the various conductivity fields tested. The same positive flux definition as in Section 4.5 is used, i.e. fluxes in the East, North and up directions are positive. It is interesting to note that the flow across the boundaries is fairly unaffected by the tested conductivity fields; the flow patterns at 450 metres depth certainly indicated more dramatic effects. The transport of salt across the boundaries show larger variations, but the basic pattern remains.

Table 4-5. Volume [l/s] and salt [g/s] flux across boundaries of a box of 2 x 2 x 0.9 km³ centred around Äspö HRL. Sensitivity to various assumptions about the conductivity field. Reference conditions are according to the data given in Chapter 2, while other cases are defined by the departure from the reference case.

Case	Boundary fluxes of volume [l/s] (top) and salt [g/s]					
	West	East	South	North	Bottom	Top
Reference conditions	1.90	-0.38	0.69	0.09	-0.01	2.87
	1.72	-1.52	1.57	0.14	-0.04	4.50
No depth-dependence on conductivity field	2.02	-0.35	0.65	0.06	-0.02	2.93
	3.87	-2.00	3.03	0.33	-0.05	8.06
Standard deviation put to zero	1.42	-0.30	0.47	-0.02	-0.01	2.21
	1.27	-1.12	1.06	-0.06	-0.24	3.38
Anisotropic conductivity	2.74	-0.41	0.57	-0.33	0.00	4.04
	2.12	-2.28	2.87	-0.41	-0.06	7.65
Transmissivities increased (10 x T)	2.93	-0.52	1.38	0.08	-0.02	4.73
	3.47	-5.20	2.18	0.05	-0.48	10.55
Transmissivities decreased (0.1 x T)	1.68	-0.33	0.42	0.10	-0.01	2.32
	1.17	-0.90	1.31	0.18	-0.30	3.03

The general conclusion from these sensitivity studies is that the flow pattern at 450 metres depth is sensitive to a modified conductivity field. As the ultimate use of the flow field is in transport calculations, it is obvious that we need to be able to determine which of the flow fields in the Figures 4-19, 4-20 and 4-21 is the more realistic one. The integrated fluxes below Äspö, as defined above, seem to be less sensitive to the various assumptions about the conductivity field.
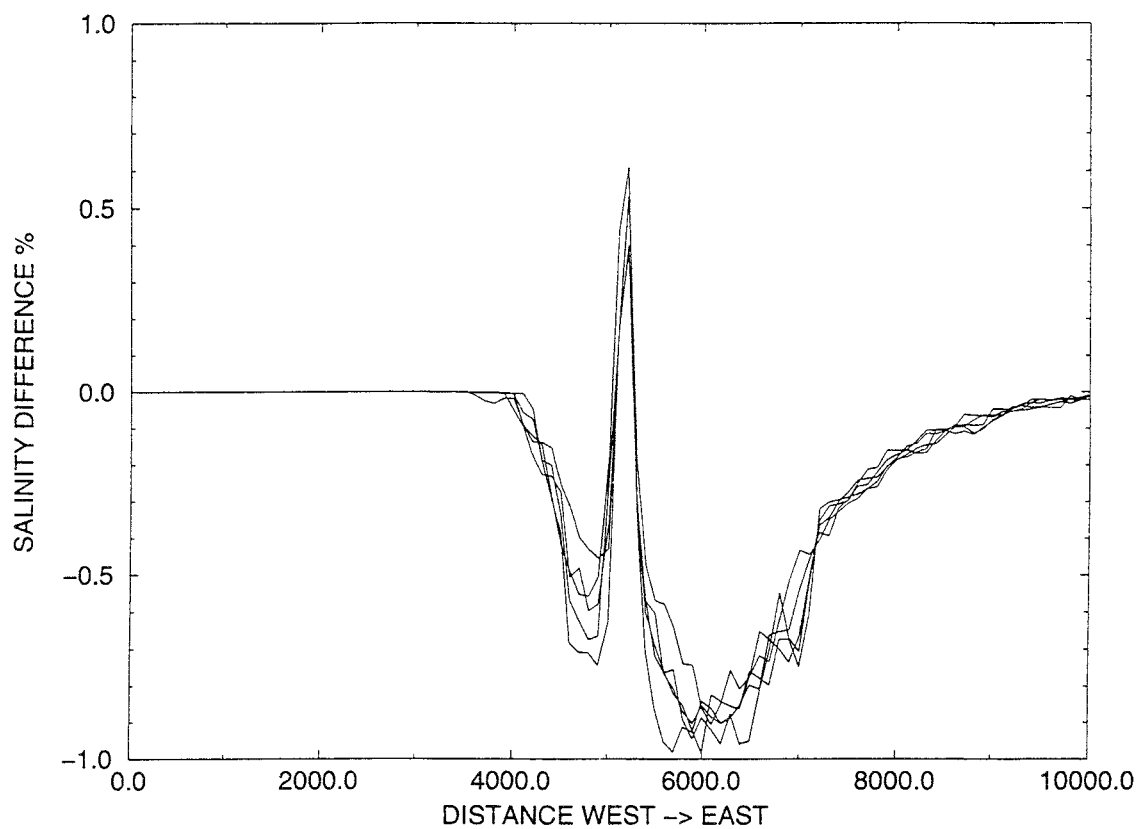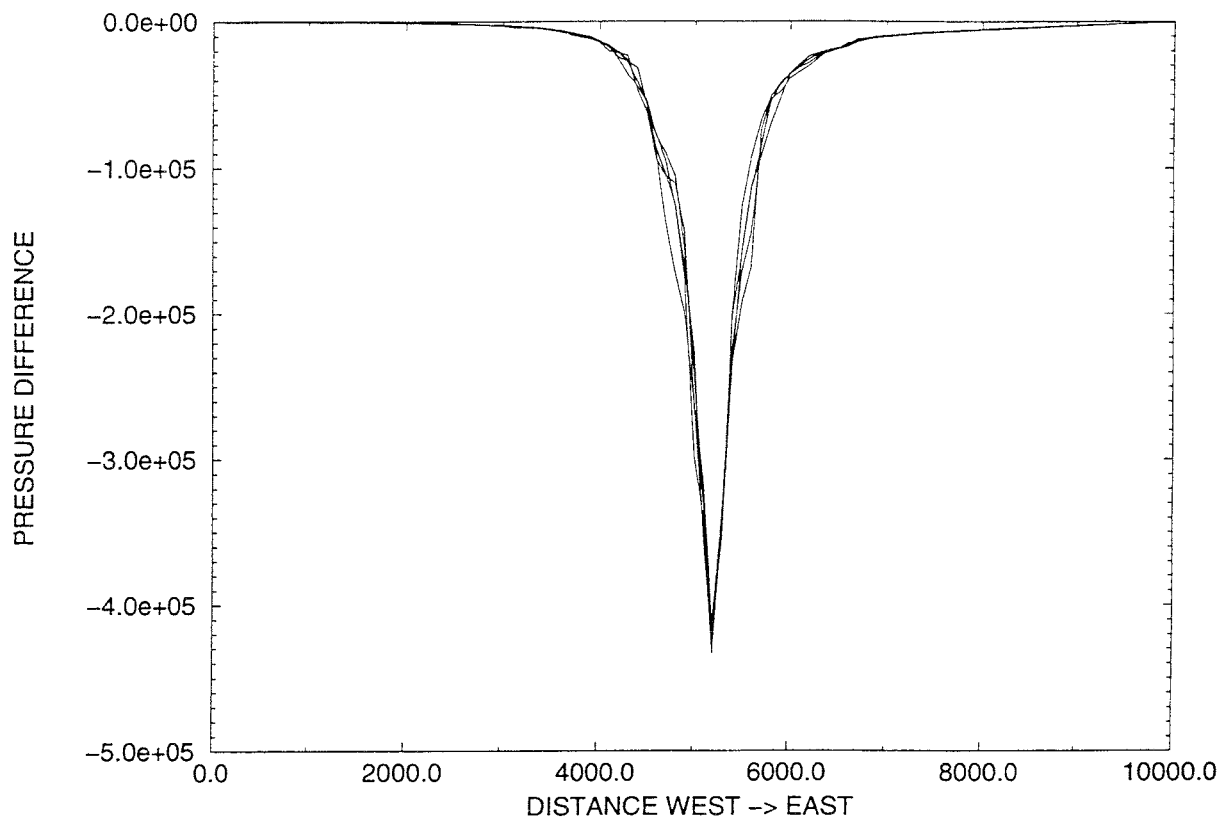
Figure 4-18. Pressure (top) and salinity difference along a west to east coordinate at 450 metres depth, through the Äspö HRL. Five realisations of the conductivity field were used to obtain the difference between natural conditions and with Äspö HRL present.
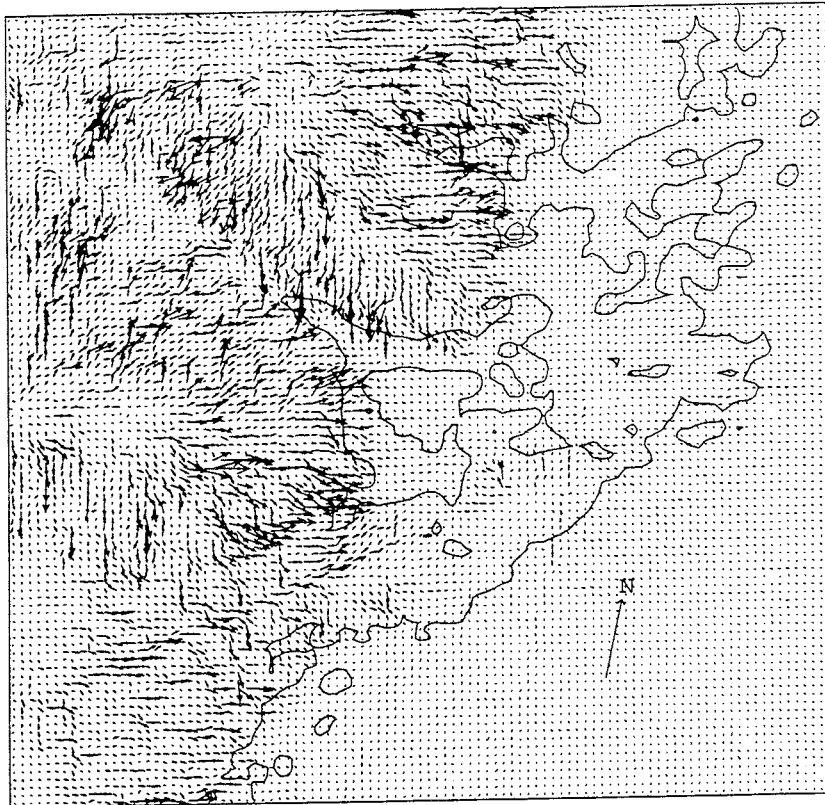
Scale: |- - - - -| 1000 m
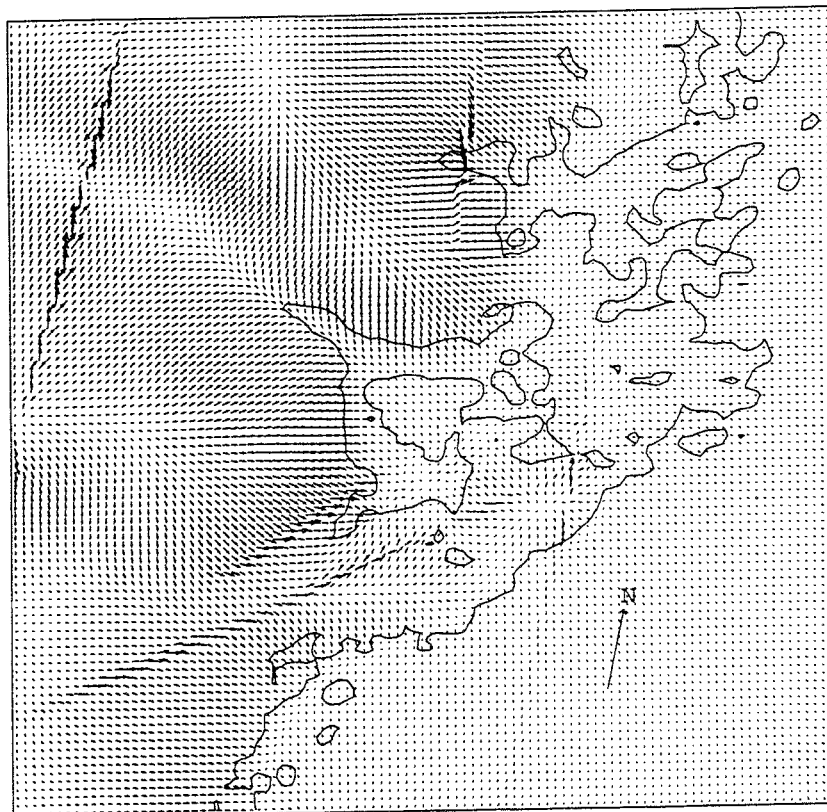
Scale: |- - - - -| 1000 m

Figure 4-19. *Horizontal flow at 450 metres. No vertical variation of background conductivity (top) and no stochastic variation of background conductivity.*

Darcy velocity scale: ———→ $2 \times 10^{-8}\, m/s.$
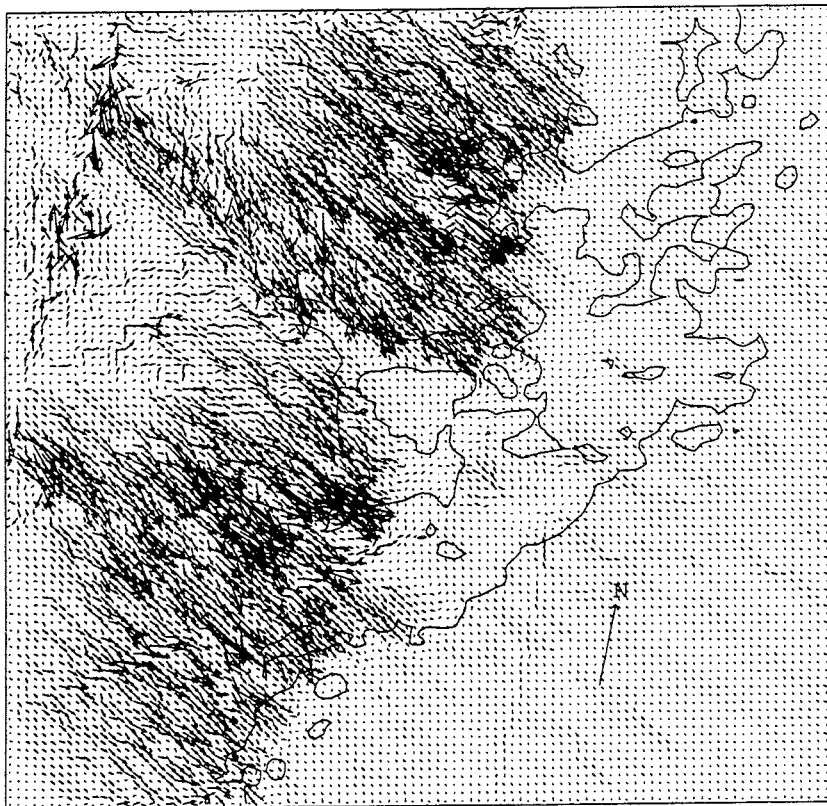
Scale: |-----| 1000 m

Figure 4-20. Horizontal flow at 450 metres with an anisotropic background conductivity.

Darcy velocity scale: ⟶ $2 \times 10^{-8} \, m/s$.
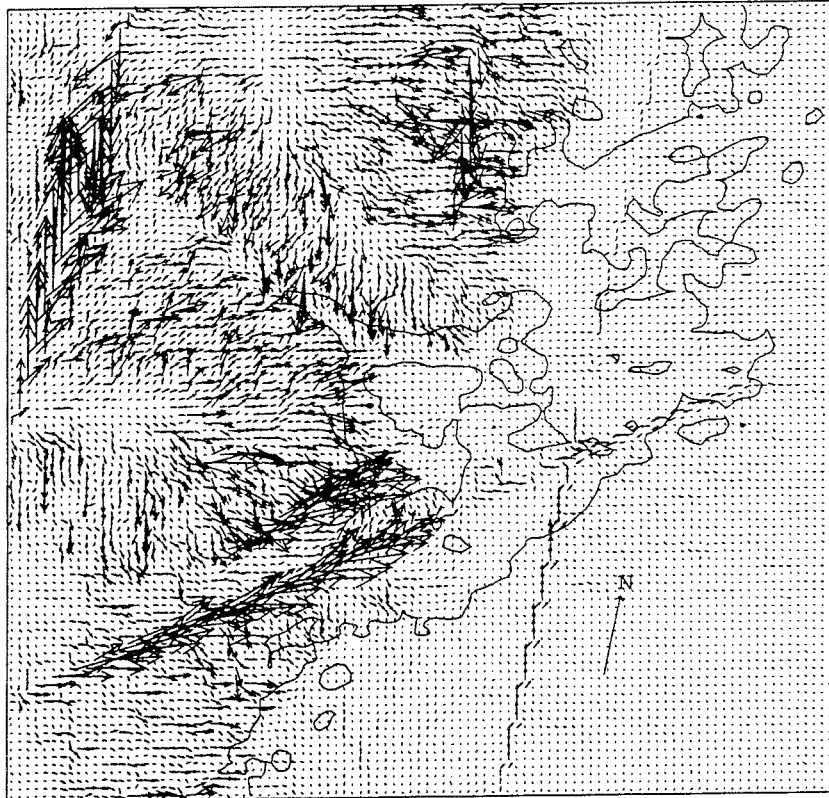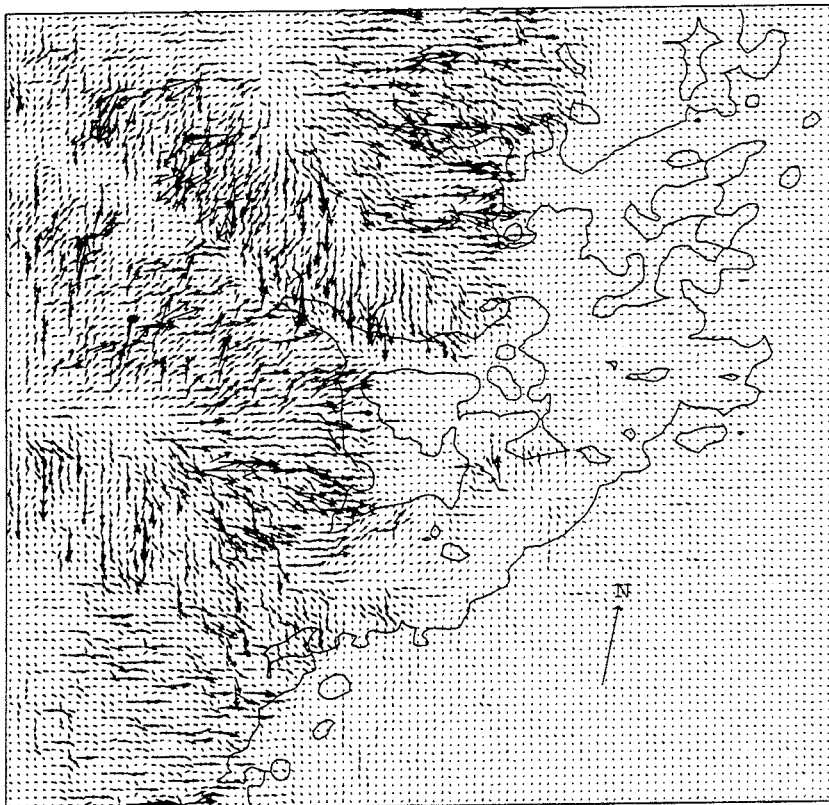
Scale: |-----| 1000 m

Scale: |-----| 1000 m

Figure 4-21. Horizontal flow at 450 metres depth with transmissivities increased (top) or decreased by an order of magnitude.

Darcy velocity scale: ⟶ $2 \times 10^{-8} m/s$.

4.7 SENSITIVITY TO THE DENSITY STRATIFICATION

In Section 3.1 it was argued that the model ought to include the effect of density stratification. It was also stated that one may question if the salinity field, which is the cause of density stratification, will ever be in a steady state. In a safety assessment of a repository we need to consider timescales of the order 100 000 years; during this time span we may even have a uniform density to a depth that exceeds the expected repository depth.

In order to get a rough estimate of the significance of the density stratification, a set of simulations without any density stratification was performed. These simulations will be compared with the corresponding ones with density stratification. We will focus on conditions at 450 metres below Äspö, as we know that a salinity stratification exists there. Another uncertainty of the predicted salinity fields is due to the dispersion process. As discussed in Section 3.2 it is not clear how it ought to be formulated mathematically, nor is the significance of the process clear. Some calculations that hopefully will shed some light on these questions will also be presented in this section.

In Figure 4-22 the flow field at 450 metres depth, with and without density stratification, is shown. As discussed earlier, we have fresh water North and West of Äspö at this depth, which means that the results should be similar in these regions. This is also found in the simulations. Below Äspö there is however significantly lower flow when stratification is present. The flow field in an East-West vertical section through the Äspö HRL is shown in Figure 4-23. When no density stratification is present the groundwater from Laxemar can penetrate very deep and end up below Äspö through the fracture zones SFZ12 and SFZ07. The density stratification will effectively limit all flow below, say, 1 000 metres and hence produce a rather different solution.

A key question in a safety assessment study is the transport time and path from a repository to ground level. In order to study this problem, and its relation to density effects, a grid of marked fluid elements was placed at a depth of 450 metres below Äspö, see Figure 4-24. To be able to carry out this particle tracking simulation one needs to estimate the pore velocity from the Darcy velocity. A porosity of 10^{-4} was assumed for this purpose. The simulation did not include any small scale dispersion effects or other retardation mechanism. The particle distributions, for the two cases, after 10 years can be studied in Figure 4-24. We see that significantly more particles have reached ground level when no density stratification is present. After 100 years all particles have reached ground-level for both cases (only the case without stratification is shown in the

figure). Obviously, there is a certain exchange also for the case with density stratification. In another simulation (not displayed in figures) the particles were placed at about 1 000 metres depth and tracked for 100 years. For this case all particles had reached ground level if no density stratification is present, while no particles had reached ground level for the stratified case.

Possibly, there is another lesson to be learned from the particle tracking simulation. If a strong regional flow was present below Äspö one would expect the particles to have moved a substantial horizontal distance, before reaching ground level. This is not the case, as can be seen in Figure 4-24, and this indicates that the flow under Äspö is governed by local conditions. However, further studies are needed to establish the regional influence on the circulation below Äspö.

Next the significance of the dispersion process will be discussed. For all simulations presented so far, the product $\beta\Delta$ (see Section 3.2) has had the value 2.0 metres. The sensitivity to this value was tested by two simulations with $\beta\Delta$ equal to 0.0 and 100.0, respectively. The result is found in Figure 4-25. The salinity distributions should be compared with the salinity distribution for $\beta\Delta = 2.0$ metres, see Figure 4-11. It is clear that the distributions are very close for $\beta\Delta = 0.0$ and 2.0, while a value of 100.0 gives a less sharp interface between the fresh and salt water. It is not possible to say which is the more realistic solution. The salinity field may also be affected by numerical diffusion. In order to investigate this effect a simulation where the standard up-wind scheme was replaced by a higher order discretization scheme was carried out. For this run $\beta\Delta$ was put to 0.0; all dispersion is thus due to numerical effects. The result is shown in Figure 4-25. As the higher order scheme does not sharpen the salinity gradient we can conclude that numerical diffusion does not seriously affect the results.

The simulations presented quite clearly demonstrate that density stratification is a significant controlling effect in a coastal area, like the one considered. We may further conclude that the simulations presented are not strongly affected by dispersion (as used in the present study) or numerical diffusion.
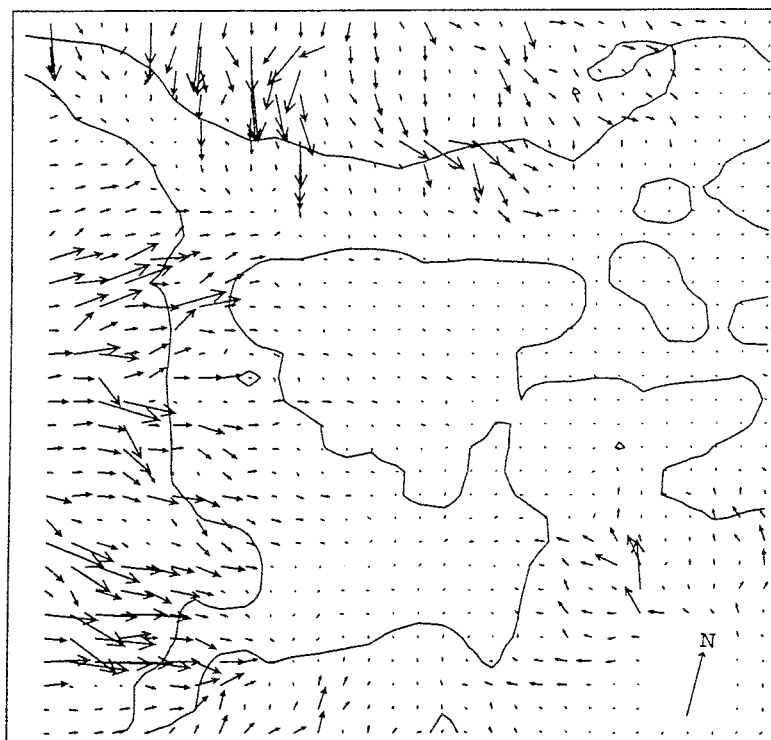
Scale: |-----| 300 m
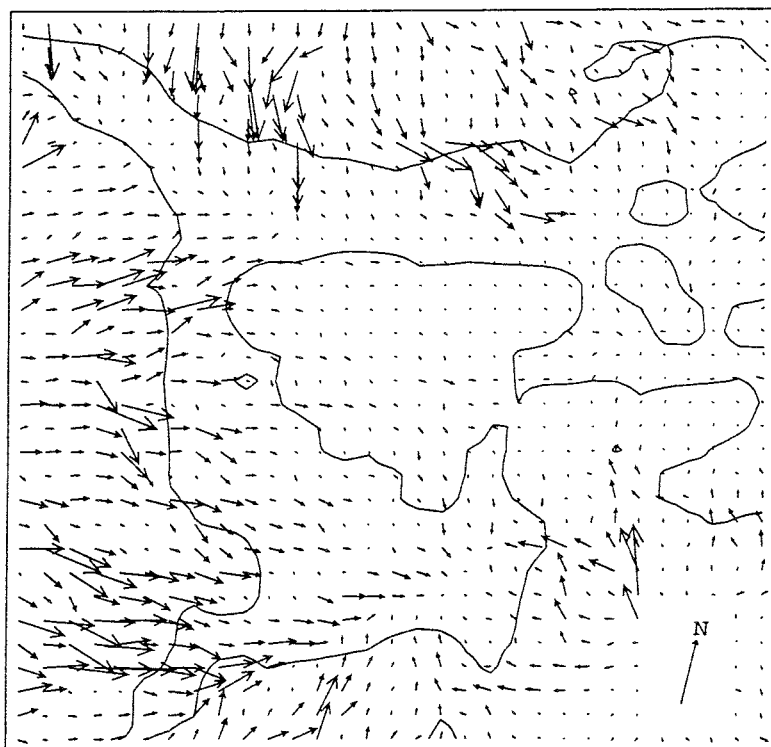
Scale: |-----| 300 m

Figure 4-22. Horizontal flow at 450 metres depth below Äspö with (top) and without density stratification present.

Darcy velocity scale: $\longrightarrow$ $5 \times 10^{-9}\, m/s$.

44

Äspö

West   East

Scale: |------| 1000 m

Äspö

West   East

Scale: |------| 1000 m
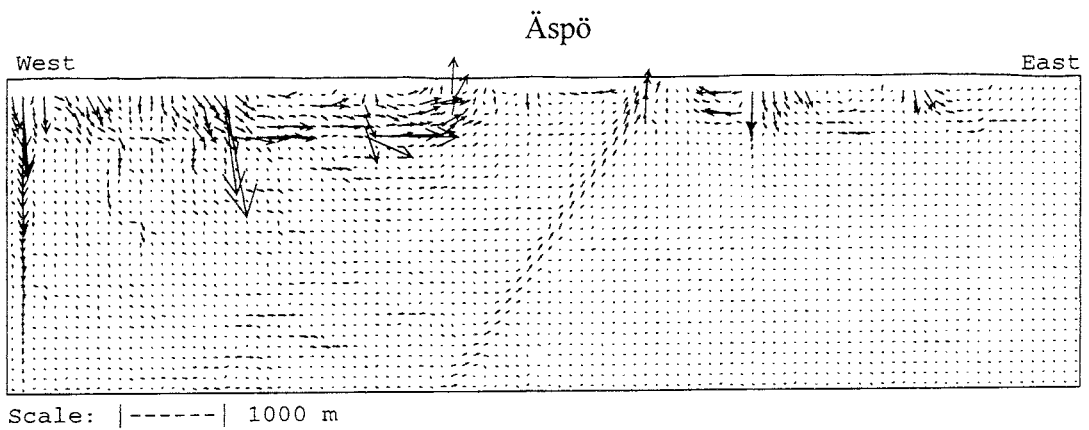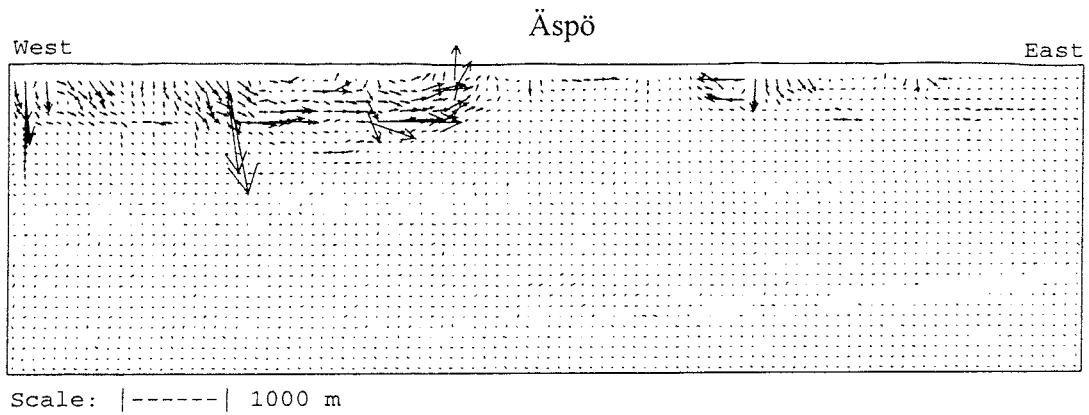
Figure 4-23. East-West sections through Äspö HRL with (top) and without density stratification present.

Darcy velocity scale: $\longrightarrow 10^{-8}$ m/s.

(Note, flow from ground to 100 metres depth not shown).
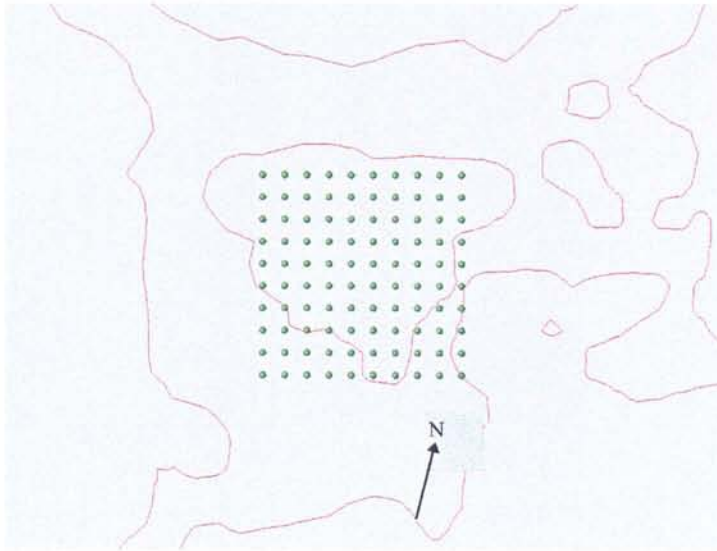
Scale: |-----| 300
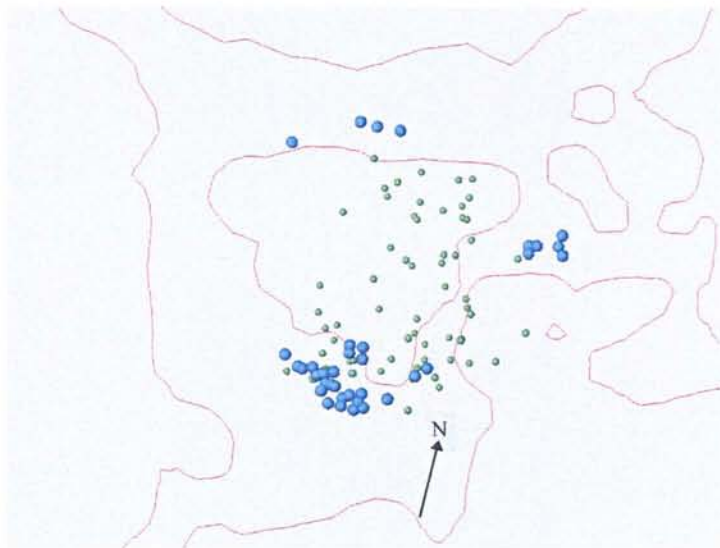
Scale: |-----| 300

Figure 4-24. *Effect of density stratification on particle transport times.*
Initial positions of particles (top).
Positions after 10 years with stratification (bottom).
Big blue particles are close to ground level, while smaller ones are at deeper levels.
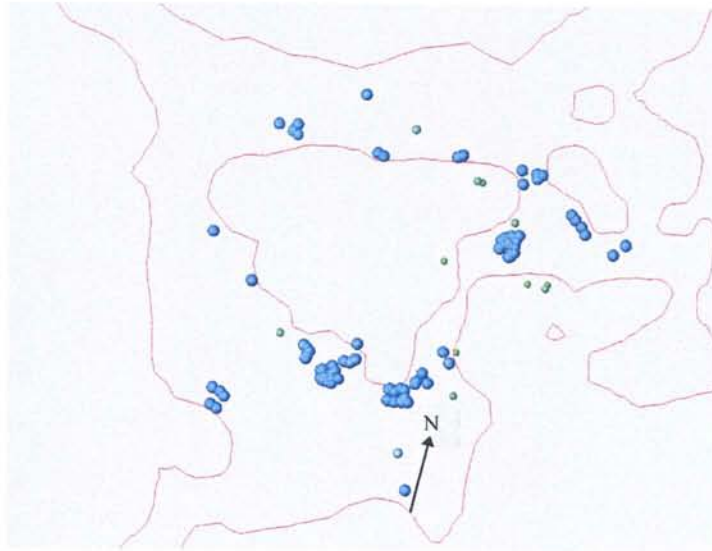
Scale: |-----| 300 m
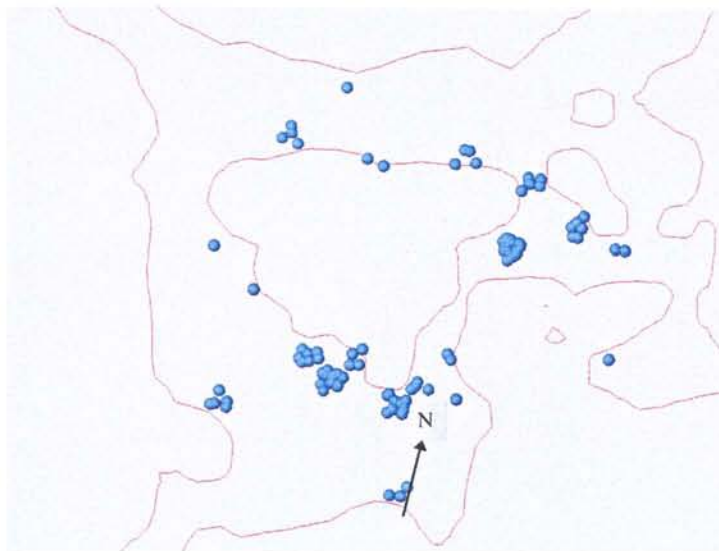
Scale: |-----| 300 m

Figure 4-24 cont. *Particle positions after 10 years (top) and after 100 years, both without density stratification present.*

47

West   Äspö   East

Scale: |------| 1000 m

Äspö

West   East

Scale: |------| 1000 m

West   Äspö   East

Scale: |------| 1000 m

Figure 4-25. *Dispersion of salt. Salinity distributions for* $\beta\Delta = 0.0$ *(top) and* 100.0 *(middle). Bottom figure based on higher order scheme and* $\beta\Delta = 0.0$.

48

5 DISCUSSION

A numerical simulation should ideally "capture the essence" of a problem and still not be too complex. In the present study it is believed that the groundwater table and the density stratification are two such essential factors that should be included in the model formulation. The reason that these two factors are emphasised is that they to a large extent govern the flow at repository depth below the island of Äspö. Relaxation of other simplifying assumptions (for example uniform recharge, vegetation and soil properties) is of interest if they significantly change the groundwater table. A practical problem is however that we do not know how to prescribe non-uniform recharge, vegetation or soil properties and we do not have observations of the groundwater table that can be used to confirm that we improve our model formulation.

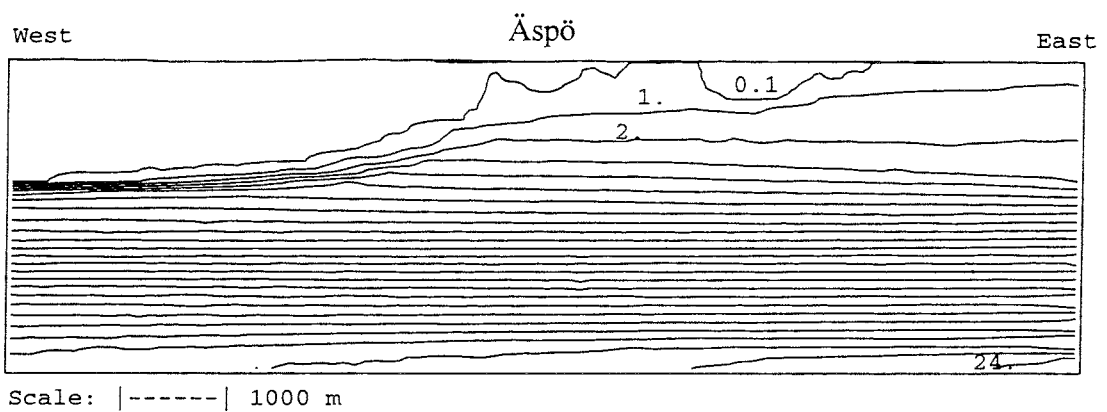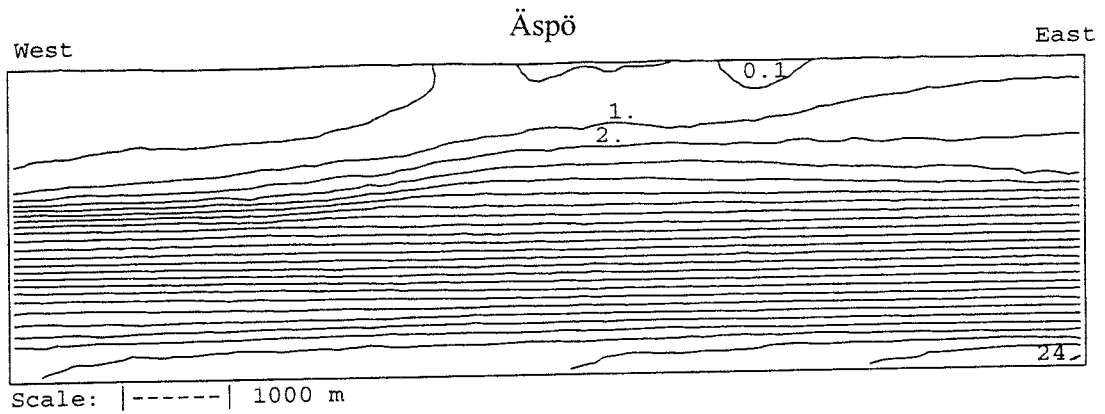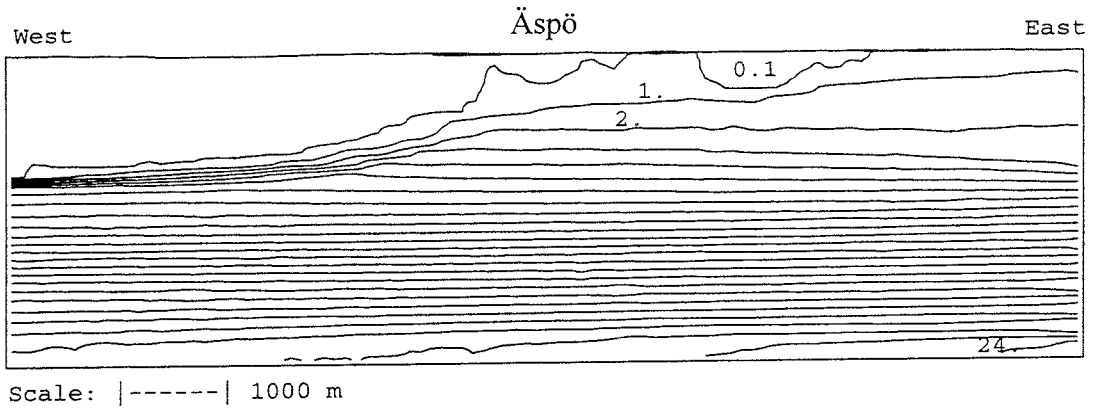When discussing "an appropriate model formulation" it is thus essential to have both the objective of the study and the available data in mind. These guide-lines have been used in the present study and it is believed that the model formulation "captures the essence of the problem" and is well balanced with respect to available data for input, calibration and verification.

A numerical groundwater model can also be viewed as a synthesis of conservation laws, empirical formulae, material properties and other data obtained from field investigations. This view is useful when discussing possible improvements of model elements. Based on experiences from the present work, the following ideas are offered for consideration when model improvements are to be discussed:

- Conductivity field. Improved knowledge about fracture zone transmissivities and rock block conductivities is the main key to increased accuracy in model predictions. The sensitivity studies presented in this report clearly demonstrate this point.

- Surface hydrology. In this report precipitation minus evapotranspiration has been set to 200 mm/year and the top four cell layers ($\approx$ 15 metres) have got their conductivities from a calibration. We may question if 200 mm/year is the best value for groundwater recharge and if a spatially non-uniform value can be estimated. It would further be useful to have some guidelines, based on field data or "general knowledge", about the near ground conductivity.

- Calibration. The accuracy of a groundwater model is to a large extent determined by the outcome of the calibration process. The model presented has been calibrated, using measured groundwater levels and salinity distributions, but further and more detailed calibration studies would be beneficial.

These are the main topics, considered to be essential for improving the model.

6 CONCLUDING REMARKS

The objective of the study presented has been to understand how the regional groundwater flow and density stratification affect the conditions below the island of Äspö. Both natural conditions and the situation with the Äspö HRL present have been considered.

It is the authors view that the regional groundwater model developed and applied, provides a realistic and consistent picture of the area studied. The main arguments for this statement are:

- The mathematical formulation of the model is based on relevant conservation laws and embodies all physical processes believed to be important for the problem considered. The importance of gravitational forces is in this context emphasised.

- A high resolution grid, which resolves topographical features and at the same time can simulate the effect of the Äspö HRL, is used.

- Transmissivities and conductivities used in the model are based on field data.

- The model has been calibrated, using measured groundwater levels and salinity distributions, with good result.

- A range of sensitivity studies has been carried out. These demonstrate that the model responds to variations in input data, for example the conductivity field, in a realistic way.

The model can thus be used to generate boundary conditions for a site scale model. The basic objective, to account for the regional influence in a site model, can hence be achieved.

7. REFERENCES

Bear J, Verruijt A, 1987. Modelling Groundwater flow and Pollution. D. Reidel Publishing Company, Dordrecht, Holland.

de Marsily G, 1986. Quantitative Hydrogeology. Academic Press, Inc.

Ghassemi F, Jakeman A.J, Jacobson G, Howard K.W.F, 1996. Simulation of seawater intrusion with 2D and 3D models: Nauru Island Case study. Hydrogeology Journal, v.4, no. 3, pp 4-22.

Oldenburg C.M, Pruess K, 1995. Dispersive transport dynamics in a strongly coupled groundwater-brine flow system. Water Resources Research, Vol. 31, No. 2, pp 289-302.

Rhén I (ed), Gustafson G, Stanfors R, Wikberg P, 1997. Äspö HRL – Geoscientific evaluation 1997/5. Models based on site characterization 1986-1995. SKB TR 97-06

Spalding D.B, 1981. "A general purpose computer program for multi-dimensional one- and two-phase flow". Math. Comp. Sim., 8, 267-276. See also: http://www.cham.co.uk

Svensson U, 1995. Modelling the unsaturated zone at Äspö under natural conditions and with the tunnelfront at 2874 metres. SKB, Progress report 25-95-24.

APPENDIX A

DOCUMENTATION

CONDENSED DESCRIPTION OF GROUNDWATER FLOW MODEL.

A regional analysis of groundwater flow and salinity distribution in the Äspö area. Stochastic continuum model	
Scope: Groundwater and salinity distributions on a regional scale	
Process description Conservation of mass, volume and momentum (Darcy´s law)	
CONCEPTS	**DATA**
Geometric framework and parameters	
Domain divided into computational cells to which conservation laws are applied.	Domain size: 10 x 10 x 3 km^3 Computational grid: 360 000 cells
Material properties	
Hydraulic conductivities. Density varies with salinity.	Various assumptions about conductivity- and salinity fields are evaluated. Data from Rhén et al (1997).
Spatial assignment method	
Stochastic conductivity for the good rock, deterministic fracture zone transmissivities.	Data from Rhén et al (1997).
Boundary conditions	
Zero flux condition on bottom and vertical boundaries facing land. Prescribed pressure and salinity at vertical boundaries facing the Baltic sea and below sea. Prescribed recharge on land.	Data from Rhén et al (1997).
Numerical tool PHOENICS **Output parameters** Flux, pressure, salinity, density	

SKB-ÄSPÖ HARD ROCK LABORATORY

Documentation of numerical simulation by Urban Svensson (US) 1997-04-11
                                                    Name   Date

OBJECT
SKB purchase order no:82030-96-200
Title of SKB purchase order: SR97 - Regional geohydrologisk analys av
                                        Äspöområdet

Author of report: US   Company: CFE AB
Operator of computer and software: US   Company: CFE AB

COMPUTER
Name and version: Silicon Graphics, Indy,R4000/SC.

SOFTWARE
Operative system: IRIX 5.3
Code name: PHOENICS 2.1   Main manual: On line
Program language: FORTRAN
Compiler: F77 for IRIX 5.3
Postprocessor name: Manual:
Postprocessor name: PHOTON   Manual:
Subroutine: Report:
Subroutine: Report:
Subroutine: Report:

CODE VERIFICATION
Distributor: Not compiled in a single report.
Report/article:
Report/article:
Other verification
Report/article: See Svensson (1995) and (1991), as referenced in this report.
Report/article:

INPUT DATA
Ref: Rhén et al (1997), see reference list.
Ref:
Ref:
Ref:
Datafile name: Data of issue: Stored at:
Datafile name: Data of issue: Stored at:
Datafile name: Data of issue: Stored at:

RESULTS
Report/article: All given in this report.
Report/article:
Data file name: Stored at:
Data file name: Stored at:

APPENDIX B

DETERMINATION OF CELL WALL HYDRAULIC CONDUCTIVITIES ACCOUNTING FOR FRACTURE ZONES.

1	# INTRODUCTION

In a numerical simulation model the computational domain is divided into computational cells. For the present problem the number of such cells is normally in the range 10^4 - 10^5. A hydraulic conductivity is needed in each of the six cell walls of a cell.

Fracture zones will strongly influence the cell wall conductivity if the fracture intersects the cell wall. The number of fracture zones, or deterministically treated fracture zones, is of course not a fixed number but depends on the actual site and how detailed the geological survey is done. Typically we may however need to treat 10-20 fracture zones in a deterministic manner.

The above cited numbers of cells and fracture zones indicate that an effective method is needed for determining the cell wall conductivities from the data on fracture zones, i.e. location and transmissivity. The objective of this appendix is to outline the mathematical basis of such a method.

2	# THE COMPUTATIONAL GRID AND FRACTURE PLANE

The method will be derived for a general topologically cartesian grid i.e. each grid cell has six cell walls but orthogonality is not required. This grid is in PHOENICS called a body-fitted grid (BFC) as it can be squeezed and stretched to fit a complex domain, see Figure B-1a. The fracture is supposed to be fully described by the coordinates of three corners and the transmissivity. A fracture of a rectangular form has to be considered as two triangular fractures as we can not generally assume that four points lie in the same plane. This note also applies to the cell wall as the four points determining the cell wall can not be expected to lie in the same plane. For this reason the cell wall is considered to consist of two triangular parts.

The mathematical problem is thus to determine the length of intersection of two triangular planes of limited extension, see Figure B-1b.

3	# DETERMINATION OF LENGTH OF INTERSECTION

The length of intersection will be determined by applying some elementary vector algebra. In addition to subtracting and adding vectors we will use the scalar product and the cross product. The technique to be used is to find constraints and conditions for the intersection of the two planes.

The two planes are shown in Figure B-2, where the coordinates for corner points have also been introduced. The vectors shown are calculated initially for each fracture for later use. In order to introduce the vector technique used it will be explained how the vectors are calculated. $\vec{S_1}$, $\vec{S_2}$ and $\vec{S_3}$ are obtained by subtraction of relevant corner coordinates of the fracture; for example $\vec{S_1}$ = (XF$_2$ - XF$_1$, YF$_2$ - YF$_1$, ZF$_2$ - ZF$_1$).

The vector $\vec{S_4}$ is the cross product of $\vec{S_1}$ and $\vec{S_2}$ and thus represent the area of the triangle and points according to the right handed convention. The three vectors $\vec{e_1}$, $\vec{e_2}$ and $\vec{e_3}$ are obtained as the cross product between $\vec{S_4}$ and $\vec{S_1}$, $\vec{S_2}$ and $\vec{S_3}$ respectively.

3.1 DO THE PLANES INTERSECT AT ALL?

If the two planes do not intersect the length of intersection is obviously zero and that part of the cell wall does not need any further consideration. An answer to this question can be found by studying the scalar product between $\vec{S}_4$ and the vectors formed by one fracture corner and the three cell wall corners.

By noting that the scalar product changes sign at an angle between the vectors of 90°, it is found that: "if all three vector products have the same sign the two planes do not intersect".

3.2 DO THE TRIANGLES INTERSECT?

Above we determined if the cell wall triangle intersects the fracture plane assuming the latter to be infinite. Next we bring in the limited extent of the fracture plane into account. In Figure B-3 it is illustrated how the cell wall triangle intersects the fracture plane but not the fracture and also how the two triangles intersects partly or fully. To be able to determine the length of intersection we first need to determine the points of intersection D and E, see Figure B-3. How this is done is illustrated in Figure B-4. The scalar product between the vector formed by ① and A and $\vec{S}_4$ gives a distance proportional to AA. The scalar product between the vector formed by ① and B and $\vec{S}_4$ gives a distance proportional to AB. By use of congruent triangles we may then determine the point D and by applying the same procedure to A and C we can determine point E.
In our ambition to determine the length of intersection we will first determine if they intersect at all. If the scalar product of the vector formed by ① and D, see Figure B-2, and $\vec{e}_2$ is less than zero we know that point D lies outside the fracture edge perpendicular to $\vec{e}_2$. If also point E lies outside that edge we know that the triangles do not intersect. By applying the same principle to all three fracture edges we can exclude the cases where the triangles do not intersect.

3.3 LENGTH OF INTERSECTION

We now know that the triangles do intersect and want to determine the length of intersection. The maximum length is, see Figure B-3, given by the two points D and E, but the triangles may also intersect only partly. If this is the case the length is determined by the two scalar products described in 3.2. If these have different signs the triangles intersect partly and the length can be determined by a procedure similar to the one illustrated in Figure B-4 and described in 3.2. Partial intersection along the other two edges are determined in a similar fashion.

We started by excluding the case that the cell wall triangle does not intersect the fracture plane. We then excluded the case that the two triangles did not intersect and have also considered the case when the triangles intersects partly. What is left is that the triangles intersects fully which concludes the analysis.

4 CELL WALL HYDRAULIC CONDUCTIVITY

Once the length of each fracture in each cell wall has been determined it is a straightforward matter to calculate the average conductivity for the cell wall. The

conductivity for a cell wall without a fracture is first determined as a lognormally distributed conductivity with a given mean value and standard deviation. If the areas of the two triangles making up the cell wall are denoted A_1, and A_2 and conductivity without fractures k_0 the new conductivity is calculated from:

$$K = (A_1 k_0 + \Sigma \lambda_{1i} T_{1i} + A_2 k_0 + \Sigma \lambda_{2I} T_{2i}) / (A_1 + A_2)$$

where the fracture length is denoted λ and its transmissivity T.

5   CONCLUDING REMARKS

The derivation presented is intended to illustrate the principles used for determining the modification of the cell wall conductivity due to the presence of a fracture. It has not been the purpose to present a mathematical derivation.
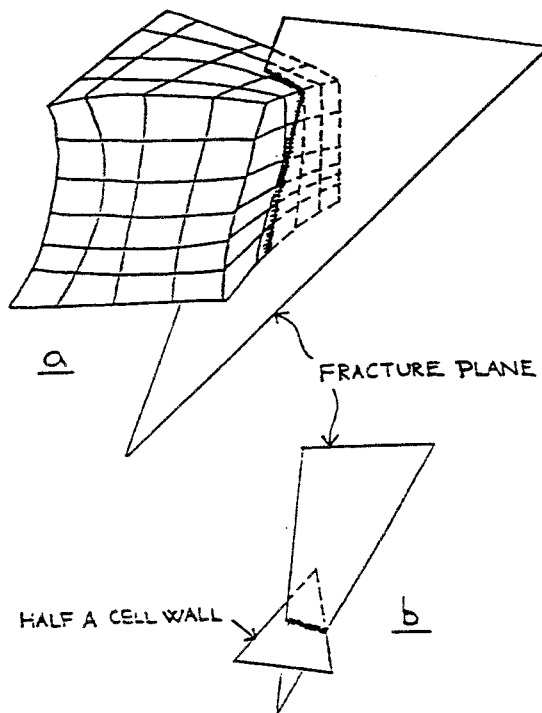

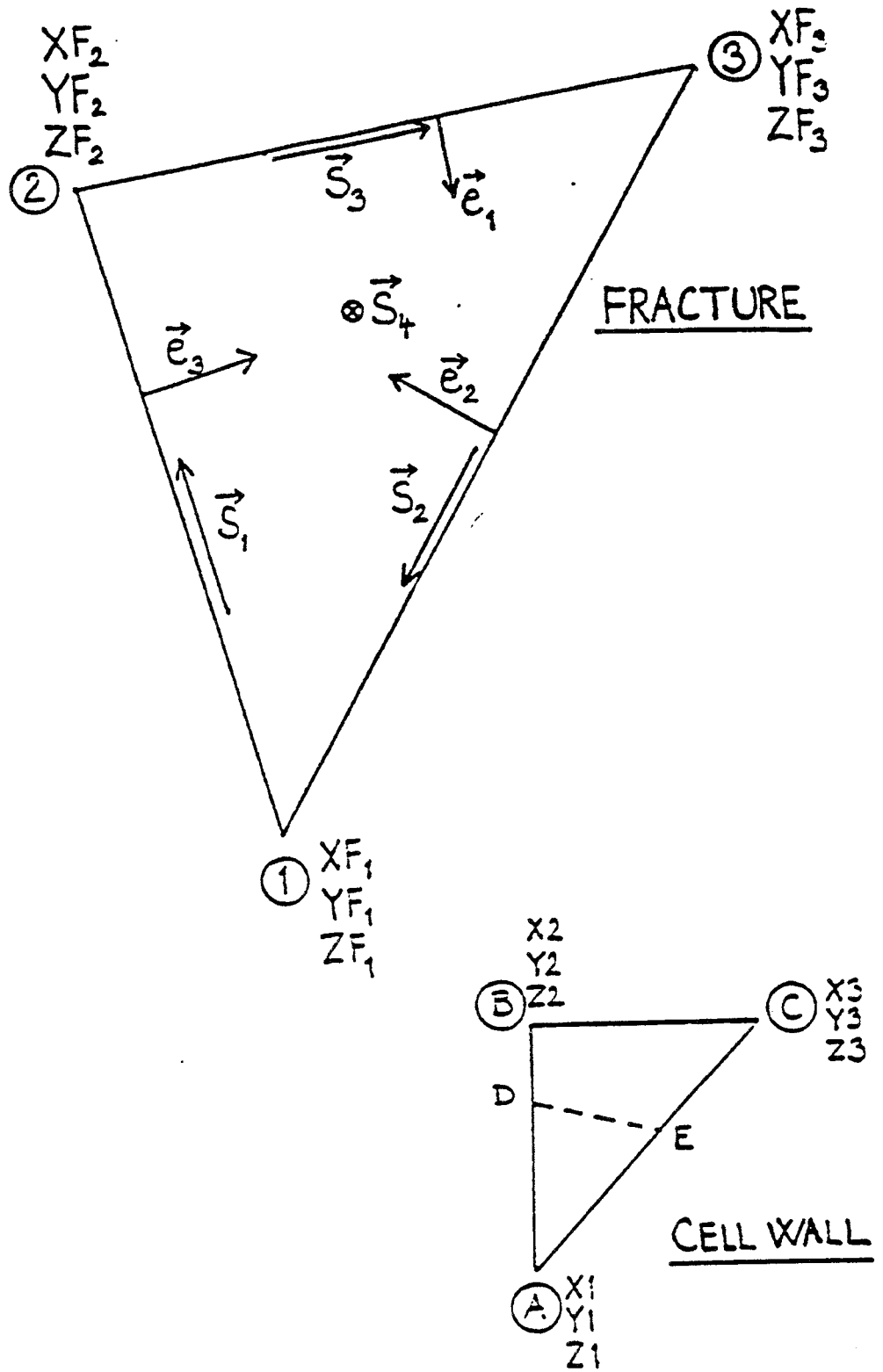Figure B-1. BFC-grid with a fracture (a) and the intersection of two triangles (b).

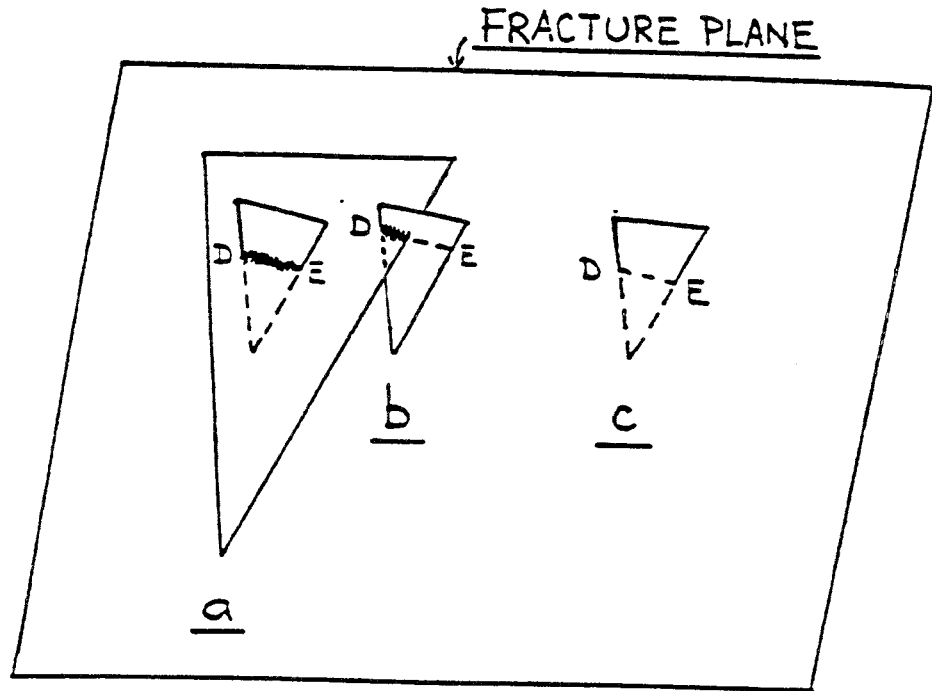Figure B-2. Definition of coordinates and vectors.

Figure B-3. Illustration of how the cell wall can intersect the fracture
plane but not the fracture (c) and how the two triangles
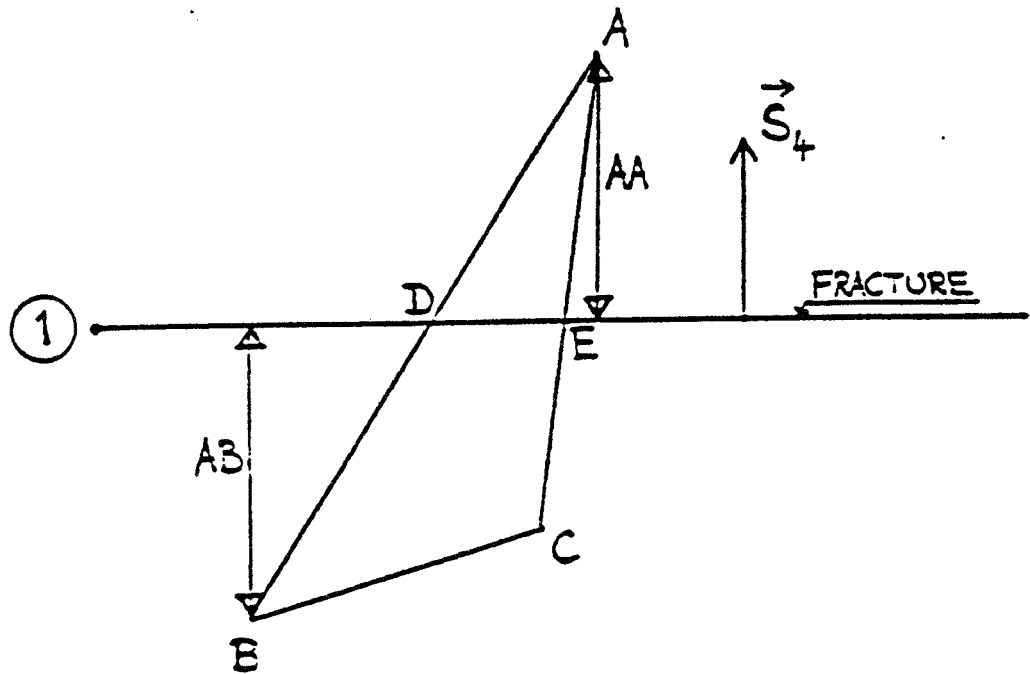intersect fully (a) or partly (b).

Figure B-4   Notation and illustration for the determination of D and E.

List of SKB reports

Annual Reports

1977-78
TR 121
KBS Technical Reports 1 – 120
Summaries
Stockholm, May 1979

1979
TR 79-28
The KBS Annual Report 1979
KBS Technical Reports 79-01 – 79-27
Summaries
Stockholm, March 1980

1980
TR 80-26
The KBS Annual Report 1980
KBS Technical Reports 80-01 – 80-25
Summaries
Stockholm, March 1981

1981
TR 81-17
The KBS Annual Report 1981
KBS Technical Reports 81-01 – 81-16
Summaries
Stockholm, April 1982

1982
TR 82-28
The KBS Annual Report 1982
KBS Technical Reports 82-01 – 82-27
Summaries
Stockholm, July 1983

1983
TR 83-77
The KBS Annual Report 1983
KBS Technical Reports 83-01 – 83-76
Summaries
Stockholm, June 1984

1984
TR 85-01
Annual Research and Development Report 1984
Including Summaries of Technical Reports Issued
during 1984. (Technical Reports 84-01 – 84-19)
Stockholm, June 1985

1985
TR 85-20
Annual Research and Development Report 1985
Including Summaries of Technical Reports Issued
during 1985. (Technical Reports 85-01 – 85-19)
Stockholm, May 1986

1986
TR 86-31
SKB Annual Report 1986
Including Summaries of Technical Reports Issued
during 1986
Stockholm, May 1987

1987
TR 87-33
SKB Annual Report 1987
Including Summaries of Technical Reports Issued
during 1987
Stockholm, May 1988

1988
TR 88-32
SKB Annual Report 1988
Including Summaries of Technical Reports Issued
during 1988
Stockholm, May 1989

1989
TR 89-40
SKB Annual Report 1989
Including Summaries of Technical Reports Issued
during 1989
Stockholm, May 1990

1990
TR 90-46
SKB Annual Report 1990
Including Summaries of Technical Reports Issued
during 1990
Stockholm, May 1991

1991
TR 91-64
SKB Annual Report 1991
Including Summaries of Technical Reports Issued
during 1991
Stockholm, April 1992

1992
TR 92-46
SKB Annual Report 1992
Including Summaries of Technical Reports Issued
during 1992
Stockholm, May 1993

1993
TR 93-34
SKB Annual Report 1993
Including Summaries of Technical Reports Issued
during 1993
Stockholm, May 1994

1994

TR 94-33
SKB Annual Report 1994
Including Summaries of Technical Reports Issued
during 1994
Stockholm, May 1995

1995

TR 95-37
SKB Annual Report 1995
Including Summaries of Technical Reports Issued
during 1995
Stockholm, May 1996

1996

TR 96-25
SKB Annual Report 1996
Including Summaries of Technical Reports Issued
during 1996
Stockholm, May 1997

List of SKB Technical Reports 1997

TR 97-01
**Retention mechanisms and the flow
wetted surface – implications for safety
analysis**
Mark Elert
Kemakta Konsult AB
February 1997

TR 97-02
**Äspö HRL – Geoscientific evaluation
1997/1. Overview of site characterization
1986–1995**
Roy Stanfors[1], Mikael Erlström[2],
Ingemar Markström[3]
[1] RS Consulting, Lund
[2] SGU, Lund
[3] Sydkraft Konsult, Malmö
March 1997

TR 97-03
**Äspö HRL – Geoscientific evaluation
1997/2. Results from pre-investigations
and detailed site characterization.
Summary report**
Ingvar Rhén (ed.)[1], Göran Bäckblom (ed.)[2],
Gunnar Gustafson[3], Roy Stanfors[4], Peter Wikberg[2]
[1] VBB Viak, Göteborg
[2] SKB, Stockholm
[3] VBB Viak/CTH, Göteborg
[4] RS Consulting, Lund
April 1997

TR 97-04
**Äspö HRL – Geoscientific evaluation
1997/3. Results from pre-investigations
and detailed site characterization.
Comparison of predictions and
observations. Geology and
mechanical stability**
Roy Stanfors[1], Pär Olsson[2], Håkan Stille[3]
[1] RS Consulting, Lund
[2] Skanska, Stockholm
[3] KTH, Stockholm
May 1997

TR 97-05
**Äspö HRL – Geoscientific evaluation
1997/4. Results from pre-investigations
and detailed site characterization.
Comparison of predictions and
observations. Geohydrology,
groundwater chemistry and
transport of solutes**
Ingvar Rhén[1], Gunnar Gustafson[2], Peter Wikberg[3]
[1] VBB Viak, Göteborg
[2] VBB Viak/CTH, Göteborg
[3] SKB, Stockholm
April 1997

TR 97-06
**Äspö HRL – Geoscientific evaluation
1997/5. Models based on site character-
ization 1986–1995**
Ingvar Rhén (ed.)[1], Gunnar Gustafson[2],
Roy Stanfors[4], Peter Wikberg[4]
[1] VBB Viak, Göteborg
[2] VBB Viak/CTH, Göteborg
[3] RS Consulting, Lund
[4] SKB, Stockholm
May 1997

TR 97-07
**A methodology to estimate earthquake
effects on fractures intersecting canister
holes**
Paul La Pointe, Peter Wallmann, Andrew Thomas,
Sven Follin
Golder Associates Inc.
March 1997

TR 97-08
**Äspö Hard Rock Laboratory
Annual Report 1996**
SKB
April 1997